AN ABSTRACT OF THE THESIS OF

Christopher J. Somes for the degree of Master of Science in Oceanography presented on June 30, 2009.

Title: Nitrogen Isotopes in a Global Ocean Biogeochemical Model: Constraints on the Coupling Between Denitrification and Nitrogen Fixation

Abstract approved:

Andreas Schmittner

We present a new nitrogen isotope model incorporated into the three-dimensional ocean component of a global Earth System Climate Model designed for millennial timescale simulations. The model includes prognostic tracers for the stable nitrogen isotopes, ^{14}N and ^{15}N, in the nitrate (NO_3^-), phytoplankton, zooplankton, and detritus variables of the marine ecosystem model. The isotope effects of algal NO_3^- assimilation, water column denitrification, and zooplankton excretion are considered as well as the input of newly fixed nitrogen by diazotrophs. A global database of $\delta^{15}NO_3^-$ observations is compiled from previous studies and compared to the model results on a regional basis where sufficient observations exist. The model is able to qualitatively and quantitatively reproduce the observed patterns such as high subsurface values in denitrification zones, the meridional and vertical gradients in the Southern Ocean, and the meridional gradient in the Central Equatorial Pacific. The observed subsurface minimum in the Atlantic is underestimated presumably owing to too little nitrogen fixation there. Sensitivity experiments show that algal NO_3^- assimilation, nitrogen fixation and water column denitrification have strong effects on the simulated distribution of nitrogen isotopes, whereas the effect from zooplankton excretion is weaker. Both water column and sedimentary denitrification also have important indirect effects on the nitrogen isotopes distribution by reducing the fixed nitrogen inventory, which creates an ecological niche for diazotrophs and stimulates additional nitrogen fixation. Water column denitrification has a strong but rather localized effect on the nitrogen isotope distribution in model versions without iron limitation of diazotrophy, in which a tight coupling of nitrogen fixation exists.

However, including iron limitation of diazotrophy inhibits a tight coupling between water column denitrification and nitrogen fixation in the Eastern Pacific and shifts the main location of nitrogen fixation from the Eastern Tropical Pacific to the Western Tropical Pacific, which results in a better agreement with $N' = NO_3^- - 16PO_4^{3-}$ and $\delta^{15}NO_3^-$ observations. Thus, our model results suggest that iron limitation of diazotrophy can modulate the feedback between denitrification and nitrogen fixation in the ocean. We speculate that a feedback response time on the centennial to millennial time scale may exist between denitrification and nitrogen fixation, producing imbalances in the global oceanic fixed nitrogen cycle, which may well have contributed to past changes of atmospheric CO_2 via the biological pump.

Nitrogen Isotopes in a Global Ocean Biogeochemical Model: Constraints on the Coupling Between Denitrification and Nitrogen Fixation

by
Christopher J. Somes

A THESIS

submitted to

Oregon State University

In partial fulfillment
of the requirements for the
degree of

Master of Science

Presented June 30, 2009

Commencement June 2010

Master of Science thesis of Christopher J. Somes presented on June 30, 2009

APPROVED:

Major Professor, representing Oceanography

Dean of College of Oceanic and Atmospheric Sciences

Dean of the Graduate School

I understand that my thesis will become part of the permanent collection of Oregon State University libraries. My signature below authorized release of my thesis to any reader upon request.

Christopher J. Somes, Author

ACKNOWLEDGEMENTS

I express sincere appreciation to my advisor, Andreas Schmittner, for introducing me to the world of oceanography and climate modeling and giving me the opportunity to work in this field for my graduate studies. Your advice and guidance has been invaluable to my growth as a scientist. I would like to thank my committee members Alan Mix and Ricardo Letelier for their helpful suggestions and comments that have aided my research and thesis. Eric Galbraith, Moritz Lehmann, Mark Altabet, and Joe Montoya have also provided useful comments that have contributed to this project.

My friends and family have provided tremendous support throughout this process. Without your encouragement and presence in my life, I would not have survived this journey.

TABLE OF CONTENTS

Page

1. Introduction..... 1
2. Model Description..... 5
    2.1 Physical Model..... 5
    2.2 Marine Ecosystem Model..... 5
    2.3 Nitrogen Isotope Model..... 15
3. Nitrogen Isotope Model Results..... 18
    3.1 Algal NO_3^- Assimilation..... 19
    3.2 Denitrification..... 20
    3.3 N_2 Fixation..... 20
    3.4 Zooplankton Excretion..... 21
4. Model Evaluation..... 24
    4.1 Southern Indian-Pacific..... 26
    4.2 Eastern Tropical North Pacific..... 28
    4.3 Central Equatorial Pacific..... 31
    4.4 Western Pacific..... 33
    4.5 North Atlantic..... 35
5. Discussion..... 38
6. Conclusion..... 43

Bibliography..... 45

Appendices..... 55
    Appendix A Anisotropic Viscosity Scheme..... 56
    Appendix B Marine Ecosystem Model..... 59
    Appendix C Nitrogen Isotope Model..... 68

LIST OF FIGURES

Figure — Page

1. Schematic of the marine ecosystem model with the nitrogen isotope parameters in color..... 9

2. Top: Vertically integrated annual sedimentary denitrification in SedDeni (SD). Bottom: Total denitrification in SedDeni and CTRL (which does not includes sedimentary denitrification) 10

3. Top: Annual dissolved Fe flux estimates from *Fan et al.*, [2006] using a constant 5% solubility. Bottom: Vertically integrated annual model N_2 fixation for CTRL, SedDeni (SD), FeLim (FeL) and SD+FeL..... 11

4. Global and regional comparison of (blue) denitrification rates and (red) N_2 fixation rates for (left) CTRL (which does not include sedimentary denitrification) and (right) SedDeni+FeL (SD+FeL) experiment..... 12

5. Annual surface $N' = NO_3^- - 16PO_4^{3-}$ in WOA05, CTRL, SedDeni (SD), FeLim (FeL), and SD+FeL..... 13

6. Comparison of annual World Ocean Atlas 2005 (WOA05) and model (SD+FeL) surface NO_3^- and subsurface O_2 14

7. Top Panel: Surface $\delta^{15}NO_3^-$ and δ^{15}N-detritus in the SD+FeL simulation. Bottom Panel: Isotope effect experiments where one isotope effect is neglected per simulation and its difference with SD+FeL is shown to illustrate its individual effect..... 22

8. Top Panel: Zonally Averaged $\delta^{15}NO_3^-$ in the Atlantic (left), Pacific (center), and Indian (right) oceans. Bottom Panel: Isotope sensitivity experiment where one isotope effect is neglected per simulation and its difference with SD+FeL is shown to illustrate its individual effect..... 23

LIST OF FIGURES (Continued)

Figure Page

9. Comparison of annual $\delta^{15}NO_3^-$ (‰) averaged over 200 m – 300 m of available observations (OBS), CTRL, SedDeni+FeLim (SD+FeL) experiment..... 25

10. Comparison of the Indian-Pacific sector of the Southern Ocean with the $\delta^{15}NO_3^-$ database (OBS) and SD+FeL. (a) $\delta^{15}NO_3^-$ vs. NO_3^-; (b) horizontally averaged (over available data south of the 2 μmol kg^{-1} NO_3^- contour) depth $\delta^{15}NO_3^-$ profiles; (c) surface $\delta^{15}NO_3^-$ with a 2 μmol kg^{-1} NO_3^- contour line (note no NO_3^- observations are below 2 μmol kg^{-1}).. 27

11. Comparison of the ETNP with the $\delta^{15}NO_3^-$ database and SD+FeL. (a) $\delta^{15}NO_3^-$ vs. NO_3^- Deficit Ratio; (b) horizontally averaged (within 10 μM O_2 contour) depth $\delta^{15}NO_3^-$ profiles including the experiment where the isotope effect of N_2 Fixation is neglected (No NFIX); (c) subsurface $\delta^{15}NO_3^-$ with a 10 μmol kg^{-1} O_2 contour line..... 30

12. Comparison of δ^{15}N-detritus (‰) with observations [*Altabet and Francois*, 1994] in the Tropical Pacific Ocean at 140°W..... 32

13. Western North Pacific zonally averaged model $\delta^{15}NO_3^-$ (‰) over 120°E to 150°E at 180 m depth compared with values recorded at the same depth in the region (boxes) at their respective latitude: (A) ~6.75‰ from *Yoshikawa et al.* [2006] at 0°N/S, 140°E - 150°E; (B) ~6‰ from *Kineast et al*. [2008] at 6°N, 125°E; (C) ~3 from *Liu et al.* [1995] at 25°N, 123°E..... 34

14. Comparison of the North Atlantic with the $\delta^{15}NO_3^-$ database and SD+FeL. (a) Horizontally averaged (over available data) depth $\delta^{15}NO_3^-$ profiles including the experiment where sedimentary denitrification is switched off (No SD); (b) subsurface $\delta^{15}NO_3^-$ in the database (OBS) and model (SD+FeL)..... 37

LIST OF APPENDIX FIGURES

Figure Page

A1. Surface viscosities in the meridional and zonal directions..... 57

A2. Annual averaged zonal velocity along 125°W using (a) an isotropic viscosity scheme, (b) the anisotropic viscosity scheme and (c) observations from *Kessler* [2006]..... 58

B1. Comparison of annual vertically integrated primary production rates of the (top) VGPM estimate [*Behrenfeld and Falkowski*, 1997] and (bottom) SD+FeL model simulation..... 67

Nitrogen Isotopes in a Global Ocean Biogeochemical Model: Constraints on the Coupling Between Denitrification and Nitrogen Fixation

Chapter 1: Introduction

The oceanic nitrogen cycle is an important component of the Earth's climate system because biologically available nitrogen (fixed N) is one of the major limiting nutrients for algal photosynthesis, which drives the sequestration of CO_2 from the surface ocean and atmosphere into the deep ocean via the sinking of organic matter (OM). Changes in this so-called 'biological pump' have been hypothesized to account for a significant amount of the glacial-interglacial fluctuations in atmospheric CO_2 [*McElroy*, 1982; *Falkowski*, 1997]. However, the relative contributions of the biological and physical pump to CO_2 variations remain controversial. The size of the oceanic fixed N inventory regulates the strength of the biological pump and hence atmospheric CO_2 concentrations.

Although the primary source and sink processes that contribute to the oceanic fixed N budget are relatively well known, the quantification of their fluxes is still associated with considerable uncertainty [*Codispoti et al.*, 2001; *Brandes and Devol, 2002; Altabet, 2007*; *Codispoti*, 2007]. Planktonic prokaryotes (diazotrophs) that can convert atmospheric N_2 gas into fixed nitrogen are regarded as the dominant oceanic source with minor contributions from riverine and atmospheric deposition. The dominant sink term is denitrification, which occurs in suboxic ($O_2 < 5$ μM) conditions in the water column and the sea floor sediments, where microbes use NO_3^- instead of O_2 as the electron acceptor during respiration. They convert NO_3^- into gaseous forms of nitrogen (N_2O and N_2) that are not readily available for uptake by most phytoplankton and can escape the ocean to the atmosphere [Codispoti and Richards,

1976]. The volume of suboxic water is affected by the temperature-dependent solubility of O_2 at the surface and its subduction to the ocean interior, as well as the amount of OM remineralization that occurs, both of which are sensitive to changes in climate. The anammox reaction may also be a significant component of the overall fixed N loss process in oxygen-depleted waters [*Kuypers et al.*, 2005 and 2006; *Thamdrup et al.*, 2006]. Minor contributions of nitrogen loss occur from sediment burial of organic matter. Thus, the global fluxes of N_2 fixation and denitrification are the most important processes that determine the balance or imbalance of the oceanic fixed N budget. However, N_2 fixation and denitrification are not completely independent processes and may in fact be closely coupled.

Denitrification creates N-deficient ($N' = NO_3^- - 16PO_4^{3-} < 1$) water that may result in an ecological advantage for diazotrophs over algae [*Tyrell*, 1999]. Thus, a negative feedback exists such that an initial perturbation, such as an increase in the global denitrification rate and the resulting decrease in the oceanic fixed N inventory, will lead to higher N_2 fixation dampening the N loss on the global oceanic fixed N inventory. However, just how tightly this coupling operates remains controversial, since other processes, such as iron limitation of diazotrophy [*Letelier and Karl*, 1996; *Falkowksi*, 1997*; Galbraith et al.*, 2004; *Moore and Doney*, 2007], can influence the interaction between denitrification and N_2 fixation.

Nitrogen isotope ratios in the water column and in sedimentary records provide constraints on fixed N sources and sinks. Nitrogen exists in the form of two stable isotopes, ^{14}N and ^{15}N. Resulting variations in N isotopic composition can be described as deviations in $^{15}N/^{14}N$ ratio from an accepted standard

$$\delta^{15}N = [(^{15}N/^{14}N) / R_{std} - 1] \times 1000 , \quad (1)$$

where R_{std} is the $^{15}N/^{14}N$ ratio of atmospheric N_2 gas. Isotope fractionation generally results in the enrichment of the heavier ^{15}N isotope in the reaction substrate, and its depletion in the product. The degree of this isotopic discrimination, or fractionation, for each process can be quantified with an enrichment factor, $\varepsilon = (\alpha - 1) \times 1000$, where α is the fractionation factor ($\alpha = {}^{14}k/{}^{15}k$), and k is the specific reaction rate for each isotope [*Mariotti et al.*, 1981].

The predominant source and sink terms of the oceanic fixed N inventory, N_2 fixation and denitrification, respectively, have their own distinct effects on the oceanic N isotope budgets. Diazotrophs are not N-limited and therefore can thrive in surface waters depleted in fixed N if sufficient phosphorus (P) and iron (Fe) are available for uptake. N_2 fixation introduces bioavailable nitrogen into the ocean which is close to the atmospheric N_2 isotope ratio ($\delta^{15}N \approx -2$ - 0‰), since little fractionation occurs during N_2 fixation [*Delwiche and Steyn*, 1970 ; *Minagawa and Wada*, 1986; *Macko et al*, 1987; *Carpenter et al.*, 1997; *Montoya et al.*, 2002].

Denitrification occurs under suboxic conditions ($O_2 < 5$ μmol/kg) in the water column and in sea floor sediments. Here, microbes use NO_3^- instead of O_2 as the electron acceptor during respiration and convert it to gaseous forms of N (N_2O and N_2), which can then escape to the atmosphere [*Codispoti and Richards*, 1976].

Denitrifiers preferentially dissimilate $^{14}NO_3^-$ leaving the residual oceanic nitrate pool strongly enriched with the heavier ^{15}N, with N isotope enrichment factors between 20 - 30‰ [*Cline and Kaplan*, 1975; *Liu and Kaplan*, 1989; *Brandes et al*, 1998; *Altabet et al.*, 1999; *Voss et al.*, 2001; *Sigman et al.*, 2003]. Note that because these estimates were derived from field studies in which the isotope effect was estimated from the total N loss, they implicitly include the effect of anammox [*Galbraith et al.*, 2008]. Sedimentary denitrification is generally limited by the amount of NO_3^- that fluxes into the reactive zones within the sediments. Therefore, it consumes nearly all of the influxing NO_3^-, barely expressing discrimination against

^{15}N [*Brandes and Devol*, 1997, 2002; *Sigman et al.*, 2003; *Lehmann et al*., 2004, 2007]. The average oceanic $\delta^{15}NO_3^-$ value near 5‰ [*Sigman et al.*, 1997, 1999] can be interpreted as the balance between the isotope effects of water column denitrification, sedimentary denitrification, and N_2 fixation [*Brandes and Devol*, 2002; *Deutsch et al.*, 2004; *Galbraith et al.*, 2004; *Altabet*, 2007].

The $\delta^{15}N$ signal in the water column and sea floor sediments is also affected by fractionation processes within the food chain. Marine algae preferentially assimilate the lighter ^{14}N into their biomass with enrichment factors estimated in the field between 4 - 15‰ [*Wada*, 1980; *Altabet et al.*, 1991; *Altabet and Fracois*, 1994; *Altabet et al.*, 1999; *Sigman et al.*, 1999; *Altabet and Francois*, 2001; *Karsh et al.*, 2003; *DiFiore et al*., 2006]. Nitrogen is not lost or gained from the ocean during algal NO_3^- assimilation but the spatial separation between net assimilation and remineralization can cause a trend of decreasing $\delta^{15}NO_3^-$ with depth. Distinguishing between the different isotope effects remains a challenge, especially in regions where multiple N-transformational processes are occurring within close proximity.

This study presents a global ocean-atmosphere-sea ice-biogeochemical model amended with a dynamic nitrogen isotope module. We provide a detailed description of the nitrogen isotope model and an assessment of its skill in reproducing present day $\delta^{15}NO_3^-$ observations. Comparison of model results with $\delta^{15}N$ observations will also be used to help quantify processes that affect the global oceanic distribution of $\delta^{15}N$. Sensitivity experiments illustrate the individual isotope effects of different N-transformational processes on the spatial distribution of the N isotopes. In combination with measurements in ocean sediments and in the water column, the model can be a useful tool to better understand variations of $\delta^{15}N$ and the nitrogen cycle in the past and present.

Chapter 2: Model Description

2.1 Physical Model

The physical model is based on the University of Victoria Earth System Climate Model [*Weaver et al.*, 2001], version 2.8. It includes a global, three dimensional general circulation model of the ocean (Modular Ocean Model 2) with physical parameterizations such as diffusive mixing along and across isopycnals, eddy induced tracer advection [*Gent and McWilliams*, 1990] and a scheme for the computation of tidally induced diapycnal mixing over rough topography [*Simmons et al.*, 2004]. Nineteen vertical levels are used with a horizontal resolution of 1.8ºx3.6º. In order to improve the simulation of equatorial currents we have increased the meridional resolution in the tropics to 0.9º (between 10ºS and 10ºN and smoothly transitioning to 1.8º at 20ºN/S), and added an anisotropic viscosity scheme [*Large et al.*, 2001]. A more detailed description of this parameterization and its effect on the equatorial circulation is provided in Appendix A. A two dimensional, single level energy-moisture balance model of the atmosphere and a state-of-the-art dynamic-thermodynamic sea ice model are used, forced with prescribed NCEP/NCAR monthly climatological winds.

2.2 The Marine Ecosystem Model

The marine ecosystem model is an improved version of the NPZD (nutrient, phytoplankton, zooplankton, detritus) ecosystem model of *Schmittner et al.* [2008] (Figure 1). The organic variables include two classes of phytoplankton, diazotrophs (P_D) and a NO_3^- assimilating algal phytoplankton class (P_O), as well as zooplankton (Z) and organic detritus (D). The inorganic variables include dissolved oxygen (O_2) and two nutrients, nitrate (NO_3^-) and phosphate (PO_4^{3-}), which are consumed by phytoplankton and remineralized in fixed elemental ratios ($R_{N:P} = 16$, $R_{O:P} = 170$). We note, though, that diazotrophs have been found to have $R_{N:P}$ as high as 50:1 (e.g.,

Letelier and Karl, [1996, 1998]). In addition to water column denitrification (Figure 2) and N_2 fixation (Figure 3), we include a parameterization of sedimentary denitrification (see Appendix B, equation B12 and Figure 2), based on the flux of organic carbon into the sea floor sediments [*Middleburg et al.*, 1996]. Since the model underestimates coastal upwelling, which drives large fluxes of organic carbon to the sea floor sediments, this parameterization is tuned to fit the global mean $\delta^{15}NO_3^-$ to observations. The complete marine ecosystem model description is provided in Appendix B. The global and basin scale rates of N_2 fixation and denitrification are shown in Figure 4. Figure 5 compares the different model simulations of N' with World Ocean Atlas 2005 (WOA05) observations, which is underestimated almost everywhere in the model. This occurs because of our too large suboxic zones and our too low N:P ratio of diazotrophs in the model. Figure 6 compares surface NO_3^- and subsurface O_2 with WOA05.

Water column denitrification is present in three main locations in the present-day oceans: the Eastern Tropical North Pacific (ETNP), the Eastern Tropical South Pacific (ETSP) and the Arabian Sea. Deficiencies in the physical circulation model cause the simulation of suboxic water to exist only in one of these locations, the ETNP (Figure 3B). The physical circulation model integrates coastal upwelling over a horizontal extent that is too large (due to its coarse resolution), which results in the underestimation of upwelling, export production, and the remineralization of OM. This bias leads to overestimated O_2 concentrations, larger than required for water column denitrification, in the ETSP and the Arabian Sea. However, suboxia in the so-called "shadow zone" of the ETNP is captured better and investigated more in Section 4.2. In the model, some water column denitrification also occurs in the Bay of Bengal and off SW Africa, which is not known to occur (Figure 2). Although the anammox reaction, which also eliminates fixed N in the water column, has been found to occur off SW Africa [*Kuypers et al.*, 2005, 2006].

Diazotroph's grow according to the same principles as algal phytoplankton (See Appendix B), but we also account for some of their different characteristics. For example, N_2 fixation breaks down of the triple N bond of N_2, which is energetically more costly than assimilating fixed N. Therefore, in the model, diazotrophs' growth rate is reduced by 50% relative to the algal phytoplankton class and it also exponentially decreases in waters cooler than 20°C (their growth rate is assumed to be zero below 15°C). However, diazotrophs are not limited by NO_3^- and will thrive in waters that are N-deficient (e.g., as a result of denitrification) after algal phytoplankton have depleted remaining surface NO_3^- and where sufficient PO_4^{3-} is available. Denitrification, and the propagation of N-deficient waters into the shallow thermocline by physical transport processes, therefore creates an ecological niche for diazotrophs [*Tyrell*, 1999].

One of the most important and best studied diazotrophs, *Trichodesmium*, also has large iron (Fe) requirements for growth [*Sanudo-Willhelmy et al.*, 2001]. Diazotrophs may depend on aeolian Fe deposition in oligotrophic waters because deep pycnocline inhibits upward mixing of subsurface Fe-replete waters into the euphotic zone [*Letelier and Karl*, 1996; *Falkowski*, 1997]. In the model including Fe limitation of diazotrophy, diazotroph's growth rate is reduced by an additional 50% where estimated rates of aeolian dissolved Fe deposition are very low (i.e., $< \sim 10$ μmol m^{-2} yr^{-1}) (Figure 3), primarily throughout the Tropical South Pacific [*Fan et al.*, 2006]. The pattern of N_2 fixation simulated in the Fe limitation of diazotrophy experiment such as high values in the tropical/subtropical North Pacific, the tropical/subtropical western South Pacific, the western tropical/subtropical South Atlantic, the tropical/subtropical North Atlantic and the Indian Ocean is mostly consistent with direct observations (See *Karl et al.*, [2002]), estimates based on the observed NO_3^- deficit and simulated circulation [*Deutsch et al.*, 2007], and results with a more complex ecosystem model [*Moore et al.*, 2007]. However, simulated N_2 fixation does

not extend northward of 20 - 25°N in the North Pacific and North Atlantic, whereas observations show N_2 fixation as far north as 35-40°N.

The fast recycling microbial loop is accounted for in the model according to the parameterization of *Schartau and Oschlies* [2003]. This includes a fast remineralization and excretion rates applied to phytoplankton and zooplankton, respectively, which recycle some of their biomass directly into NO_3^-. This parameterization accounts for the recycling through dissolved organic matter (DOM) and ammonium pools using fixed elemental ratios (N:P = 16:1). In oligotrophic waters, where primary production is mainly fueled by the recycling of N within the microbial remineralization loop (i.e., very low *f* ratio), it has been suggested that the more labile dissolved organic phosphorus (DOP), when compared to dissolved organic nitrogen (DON), cycles through the microbial loop more efficiently and is more readily available for consumption. This mechanism can help relieve diazotrophs of their P limitation [*Jackson and Williams*, 1985; *Smith et al.*, 1986; *Abell et al.*, 2000; *Wu et al.*, 2000], which is not accounted for in the model. Therefore, denitrification is the only process in the model that can create an ecological niche for diazotrophy. Thus, the simulated pattern of N_2 fixation is mostly a response to denitrification, and the transport of N-deficient waters to the surface where sufficient aeolian Fe deposition exists. Missing differential DOP/DON dynamics thus can explain why N_2 fixation is not more abundant in the oligotrophic waters of the subtropical gyres.

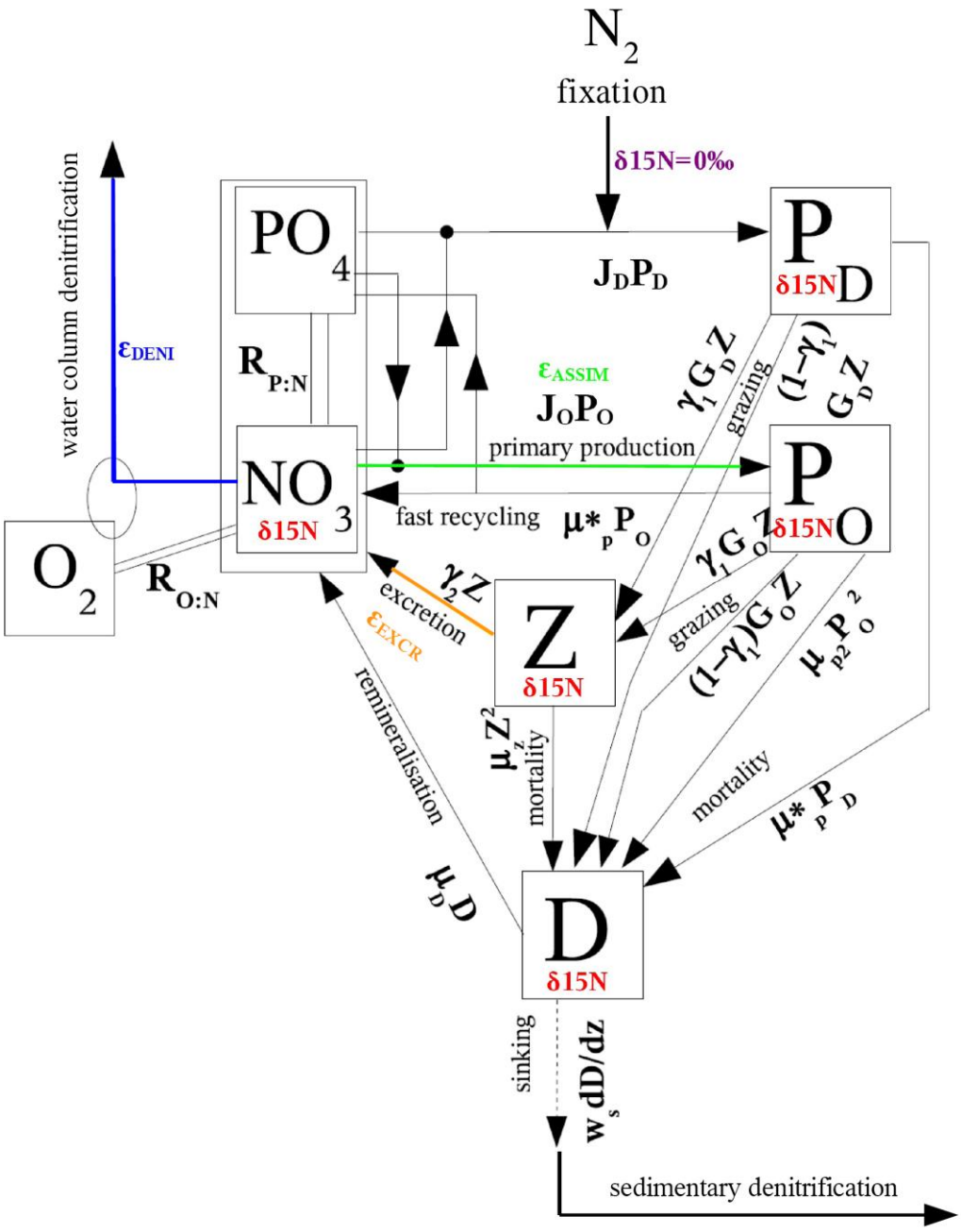

Figure 1. Schematic of the marine ecosystem model with the nitrogen isotope parameters in color.

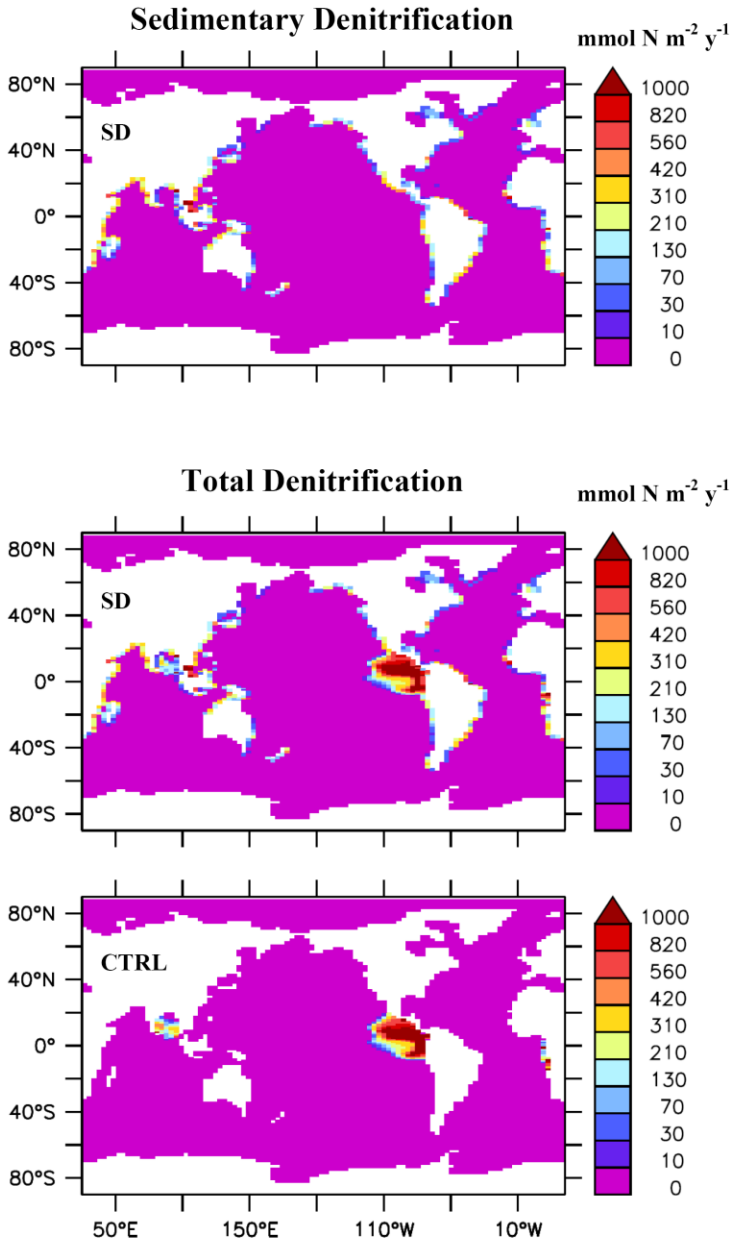

Figure 2. Top: Vertically integrated annual sedimentary denitrification in SedDeni (SD). Bottom: Total denitrification in SD and CTRL (which does not include sedimentary denitrification).

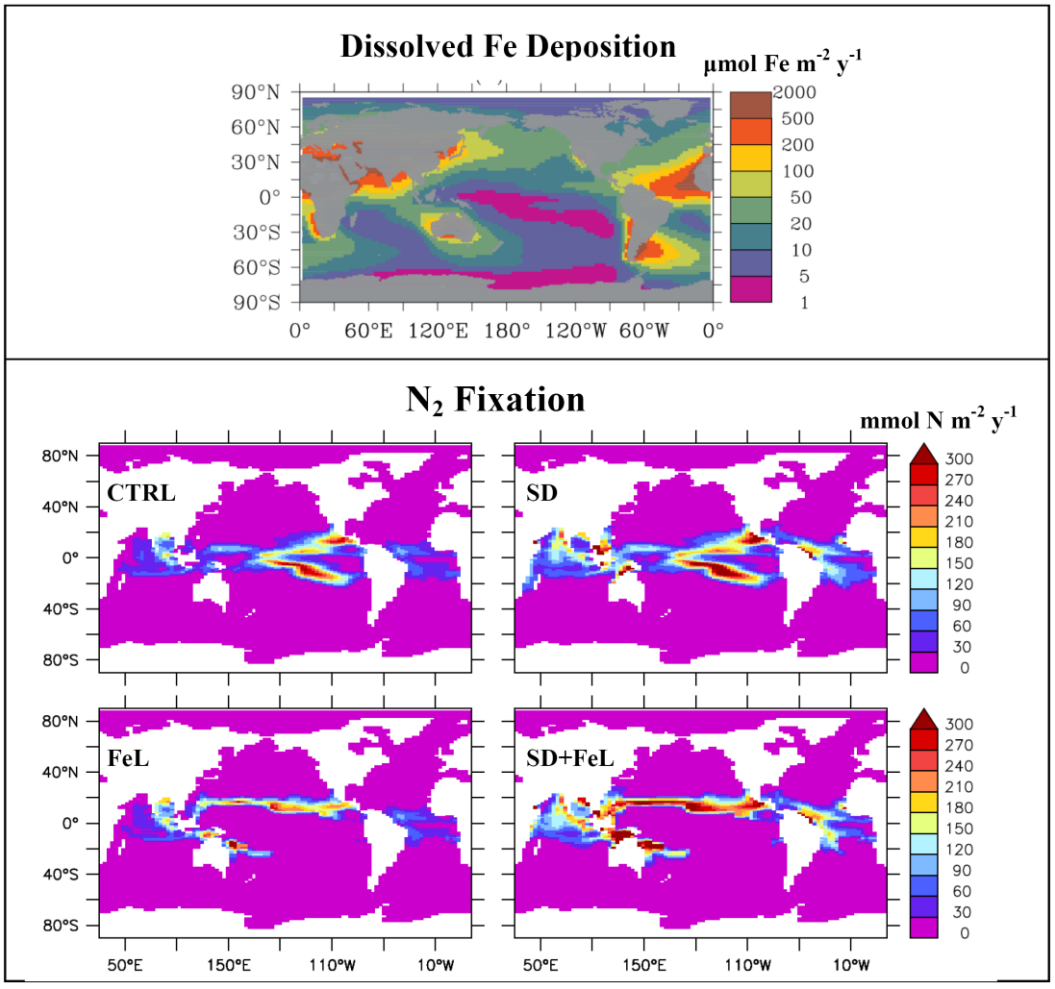

Figure 3. Top: Annual dissolved Fe flux estimates from *Fan et al.*, [2006] using a constant 5% solubility. Bottom: Vertically integrated annual N_2 fixation rates for CTRL, SedDeni (SD), FeLim (FeL) and SD+FeL.

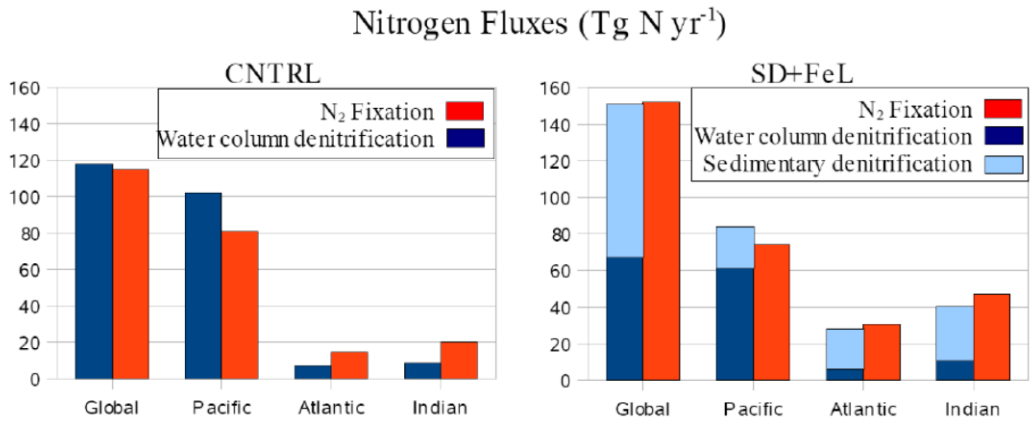

Figure 4. Global and regional comparison of (blue) denitrification rates and (red) N_2 fixation rates for (left) CTRL, which does not include sedimentary denitrification, and (right) SedDeni+FeL (SD+FeL) experiment.

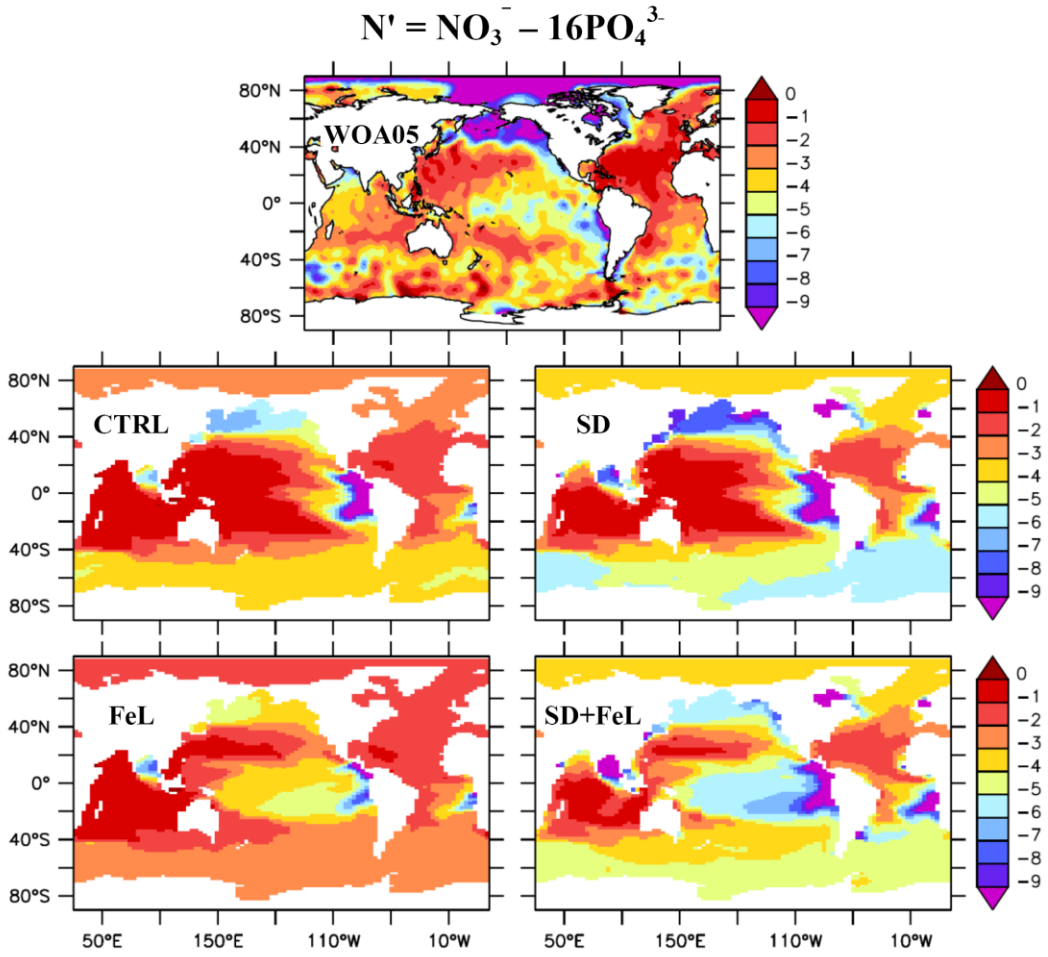

Figure 5. Annual surface N' = NO_3^- – $16PO_4^{3-}$ in WOA05, CTRL, SedDeni (SD), FeLim (FeL) and SD+FeL.

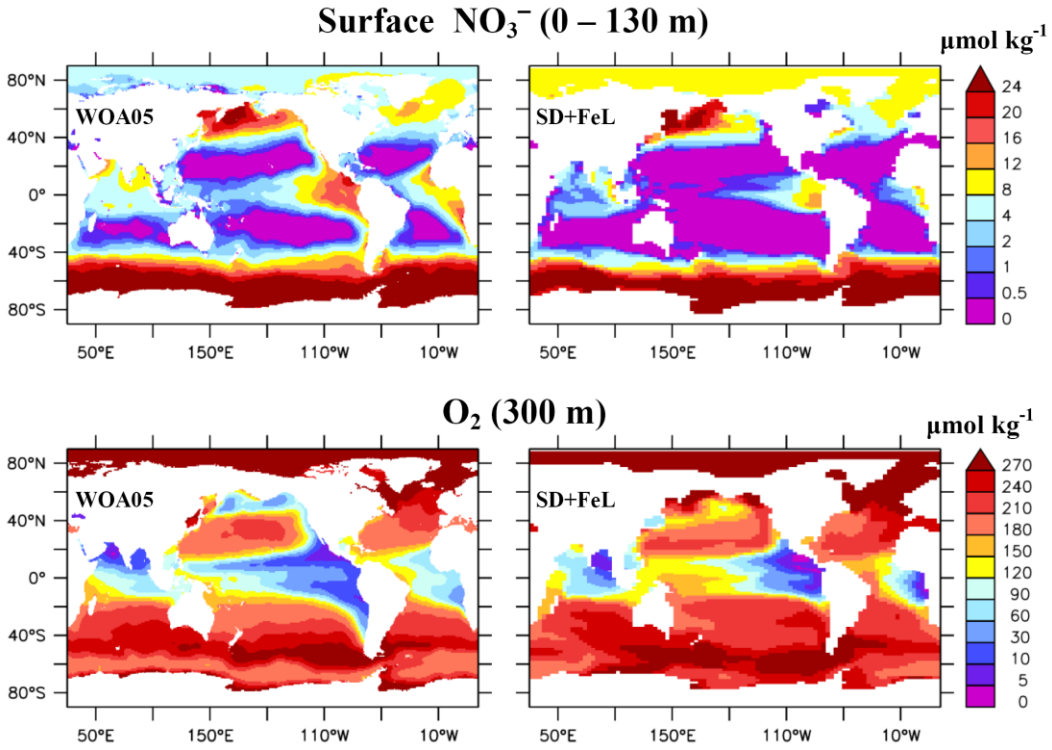

Figure 6. Comparison of annual World Ocean Atlas 2005 (WOA05) and model (SD+FeL) surface NO_3^- and subsurface O_2.

2.3 The Nitrogen Isotope Model

The nitrogen isotope model simulates the distribution of the two stable nitrogen isotopes, ^{14}N and ^{15}N, in all N species that are included in the marine ecosystem model. The prognostic variables of $\delta^{15}N$ that are embedded within the marine ecosystem model are NO_3^-, diazotrophs, algal phytoplankton, zooplankton and organic detritus (Figure 1). The "isotope effect" for each N-transformational process is referred to in the following as the effect that each process has on the oceanic isotopic N pool, which depends on the $\delta^{15}N$ value of the substrate, the process-specific enrichment factor (ε), and the degree of utilization ($u_{substrate}$) of the substrate during the reaction:

$$\delta^{15}N_{product} = \delta^{15}N_{substrate} - \varepsilon(1 - u_{substrate}) \quad (2)$$

where $u_{substrate}$ is the fraction of the initial substrate used in the reaction. For example, if all of the available substrate is consumed in the reaction (i.e., $u_{substrate} = 1$), the product will incorporate the $\delta^{15}N$ value of the substrate, nullifying any potential fractionation. However, if the rate of utilization is low (i.e., $u_{substrate} \approx 0$), the process will fractionate the isotopes near its designated enrichment factor (Table 1).

The processes in the model that fractionate nitrogen isotopes are algal NO_3^- assimilation ($\varepsilon_{ASSIM} = 5‰$), zooplankton excretion ($\varepsilon_{EXCR} = 3‰$), and water column denitrification ($\varepsilon_{WCD} = 25‰$) (Table 1). Fractionation results in the isotopic enrichment of the more reactive, thermodynamically preferred, light ^{14}N into the product of each reaction by a process-specific fractionation factor. For a detailed discussion of nitrogen isotope fractionation dynamics see *Mariotti et al.* [1981]. Although no fractionation occurs during N_2 fixation in the model, it has an important

affect on $\delta^{15}N$ by introducing relatively light atmospheric N_2 ($\delta^{15}N = 0‰$) into the oceanic fixed-N inventory. Sedimentary denitrification also has been observed to have little effect on the oceanic isotopic N pool [*Brandes and Devol,* 1997, 2002; *Lehmann et al.*, 2004]. In the model, there is no fractionation during sedimentary denitrification ($\varepsilon_{SD} = 0‰$) because denitrifiers consume nearly all of the NO_3^- fluxing into the reactive zones within the sediments and therefore barely discriminate against ^{15}N, although this is a simplification of observations [*Lehmann et al.*, 2007]. Fractionation during the remineralization of organic matter is not included in the model as well. The complete nitrogen isotope model description is provided in Appendix C.

Process	*Symbol*	*Model Enrichment Factor (‰)*	*Field Estimates (‰)* [a]
Algal NO_3 Assimilation	ε_{ASSIM}	5	4 - 15
N_2 Fixation	ε_{NFIX}	1.5	0 - 2
Excretion	ε_{EXCR}	3	3 - 6
Water Column Denitrification	ε_{WCD}	25	22 - 30
Sedimentary Denitrification	ε_{SD}	0	0 - 4

[a] see Appendix C for references

Table 1: Nitrogen Isotope Model Enrichment Factors

Chapter 3: Nitrogen Isotope Model Results

The model simulates complex spatial patterns of surface $\delta^{15}NO_3^-$ and δ^{15}N-OM sinking out of the surface (Top panels of Figures 7, 8). The $\delta^{15}NO_3^-$ and δ^{15}N-OM patterns follow similar trends but become offset as algae fractionate NO_3^- during its assimilation into their biomass. High δ^{15}N values (>15‰) exist at the poleward edges of the eastern subtropical gyres where surface NO_3^- is almost fully depleted and in regions in close proximity to suboxic zones in the Eastern Pacific, Bay of Bengal, and Eastern Atlantic (again, note that water column denitrification is not known to occur in the Bay of Bengal and Eastern Atlantic). More intermediate δ^{15}N values (4 − 8‰) are found at high latitudes and near the equator where strong upwelling occurs. δ^{15}N minima (<4‰) exist in the western tropical/subtropical ocean basins 'downstream' of denitrification zones, where sufficient aeolian Fe deposition exists for N_2 fixation to occur in the model. The processes that affect these spatial variations of $\delta^{15}NO_3^-$ and δ^{15}N-OM are described in detail below.

Figures 7 and 8 illustrate results from the full model with sedimentary denitrification and Fe limitation of diazotrophy (SD+FeL) that includes isotope effects from all processes (top panels) as well as the results from the isotope effect sensitivity experiments, which isolate the individual effects of different N-transformational processes (bottom panels) on the global distribution of δ^{15}N. This is accomplished by removing the isotope effect of one process per experiment then taking the experiment's δ^{15}N difference from SD+FeL ($\Delta\ \delta^{15}$N). For example, in the "NO_3^- Assimilation" and "Excretion" experiments, their respective enrichment factors, ε_{ASSIM} and ε_{EXCR}, are set to zero. In the "N_2 fixation" experiment, the isotope effect of N_2 fixation is suppressed by setting the diazotroph's N isotope ratio equal to that of algal phytoplankton at each location. In the "Water Column Denitrification" and "Sedimentary Denitrification" experiments, the entire process is switched off (thereby changing the global N inventory). These experiments show the indirect effect that

both denitrification processes have on $\delta^{15}N$ through stimulation of additional N_2 fixation, as well as the direct effect from fractionation during water column denitrification. In all other isotope effect experiments, the total nitrogen inventory does not change.

3.1 Algal NO_3^- Assimilation

As phytoplankton preferentially assimilate $^{14}NO_3^-$ into organic matter, they leave the residual inorganic NO_3^- pool enriched in $^{15}NO_3^-$, which can create up to 5‰ difference between surface $\delta^{15}NO_3^-$ and $\delta^{15}N$-OM, depending on the degree of surface NO_3^- utilization. This surface NO_3^- utilization effect depends on the extent to which NO_3^- is consumed at the surface with respect to its physical supply. It becomes most obvious in the "NO_3^- Assimilation" experiment (Figures 7, 8). When NO_3^- is not well utilized (i.e., supply exceeds uptake), which occurs in High Nitrate Low Chlorophyll (HNLC) regions, surface $\delta^{15}NO_3^-$ is mainly influenced by the source of $\delta^{15}NO_3^-$ being supplied to the surface. Algae will fractionate NO_3^- during assimilation in these N-replete waters so the expected 5‰ difference between $\delta^{15}NO_3^-$ and $\delta^{15}N$-OM is almost fully expressed (i.e., $\delta^{15}P_O = \delta^{15}NO_3^- - \varepsilon_{ASSIM}$ with $u_{ASSIM} \approx 0$ in Equation 2). Thus, the surface NO_3^- utilization effect in HNLC regions drives low values of $\delta^{15}N$-OM while having a smaller effect on surface $\delta^{15}NO_3^-$.

A different response is observed in oligotrophic regions where NO_3^- is nearly completely depleted at the surface. As algae draw down and fractionate the available NO_3^-, the residual surface NO_3^- becomes enriched with the heavy ^{15}N while the relatively lighter organic N sinks to greater depths. Once algae consume nearly all the remaining NO_3^- (which itself becomes enriched in ^{15}N), they acquire the same isotope value from the source water (i.e., $\delta^{15}P_0 = \delta^{15}NO_3^-$ with u_{ASSIM} approaching 1). This drives the high $\delta^{15}N$ values in both NO_3^- and OM towards the eastern poleward edges of the subtropical gyres, where NO_3^- is the most depleted in the model (Figure 7).

3.2 Denitrification

Water column denitrification only occurs at depth but its isotope effect can reach the surface due to upwelling and vertical mixing of water enriched in $^{15}NO_3^-$ (Figures 7, 8). It has a large enrichment factor and displays a very strong N isotope effect in close proximity to the simulated suboxic zones in the Eastern Pacific, Bay of Bengal, and Eastern Atlantic ("Water Column Denitrification" experiment in Figures 7, 8). The unresolved poleward undercurrents along the western continental margin of the Americas—which could, indeed, propagate high $\delta^{15}NO_3^-$ away from the subsurface suboxic zones [*Kineast et al.*, 2002]—may also be a plausible explanation as to why the simulated water column denitrification isotope effect is restricted to regions proximal to the suboxic zones. Both water column and sedimentary denitrification also indirectly lead to lower $\delta^{15}NO_3^-$ values "downstream" of denitrification zones by creating more N-deficient water, which stimulates additional N_2 fixation, and prevents a large horizontal extension of high $\delta^{15}NO_3^-$ signature originating from suboxic zones because N_2 fixation introduces much lower $\delta^{15}N$ into the ocean (See below).

3.3 N_2 Fixation

The addition of newly fixed, isotopically light atmospheric N_2 ($\delta^{15}N_2 = 0$) by diazotrophs is the reason for the low $\delta^{15}N$ values in the tropical/subtropical ocean basins. Since denitrification is the only process in the model that creates N-deficient water, and therefore an ecological niche for diazotrophs, the majority of N_2 fixation in the model occurs "downstream" of denitrification zones after algal phytoplankton have consumed all remaining surface NO_3^- and where sufficient aeolian Fe deposition exists. This low $\delta^{15}NO_3^-$ signature is evident in the subtropical North/South Pacific, the subtropical North/South Atlantic, and the Bay of Bengal ("N_2 Fixation" experiment, Figure 7).

3.4 Excretion

According to our model results, the N isotope effect of zooplankton excretion has a smaller influence on the simulated distribution of $\delta^{15}N$ in the global ocean ("Excretion" experiment, Figures 7, 8) compared to the other processes discussed above. Its effect is strongest in the model where NO_3^- is low and excretion significantly contributes to the NO_3^- pool by introducing low $\delta^{15}N$. We note that this N isotope effect is sensitive to the parameterization for excretion used in this marine ecosystem model version and needs to be further validated by observations.

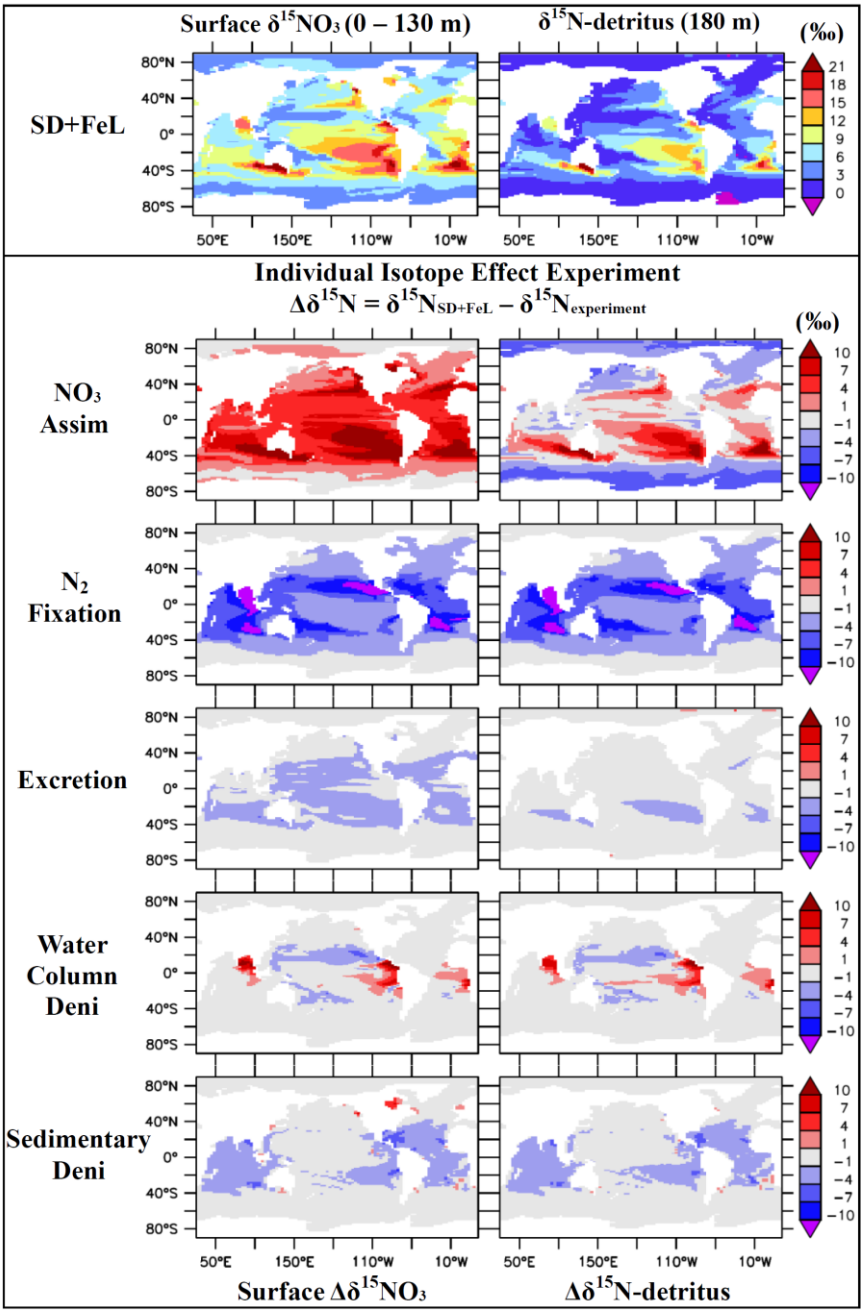

Figure 7. Top Panel: Surface $\delta^{15}NO_3^-$ and $\delta^{15}N$-detritus in the SD+FeL simulation. Bottom Panel: Isotope effect experiments where one isotope effect is neglected per simulation and its difference with SD+FeL is shown to illustrate its individual effect.

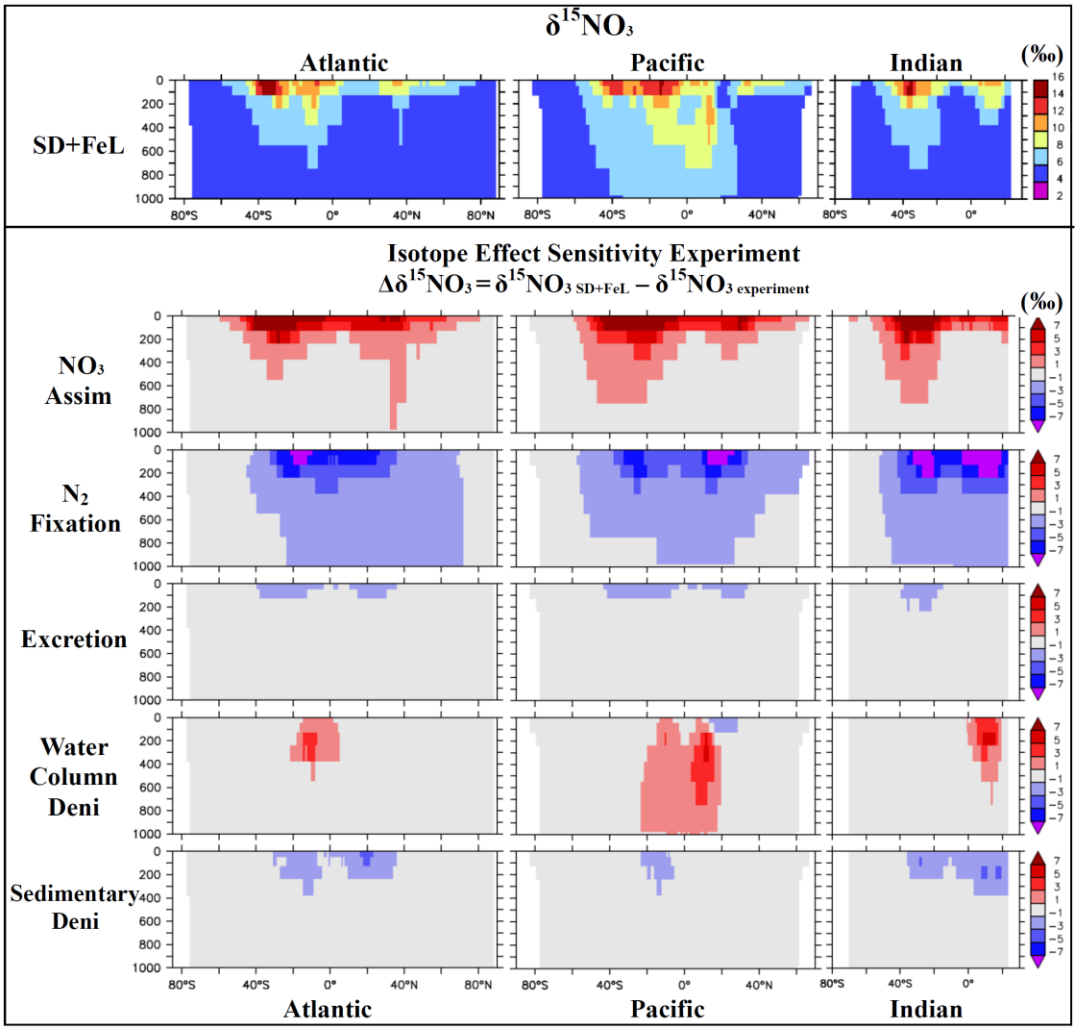

Figure 8. Top Panel: Zonally Averaged $\delta^{15}NO_3^-$ in the Atlantic (left), Pacific (center), and Indian (right) oceans. Bottom Panel: Isotope sensitivity experiment where one isotope effect is neglected per simulation and its difference with SD+FeL is shown to illustrate its individual effect.

Chapter 4: Model Evaluation

The relatively small number of $\delta^{15}N$ observations and the sparse spatial and temporal coverage make a full global model assessment difficult. However, certain regions have been sampled sufficiently enough to provide a meaningful comparison with the model results. All observations presented here are interpolated horizontally onto a 0.9° x 1.8° grid using a Gaussian weighted algorithm. The 33 depth levels are consistent with WOA05 and a linear interpolation is used for depths of missing data if nearby data exist. A global database of $\delta^{15}NO_3^-$ measurements has thus been constructed and is available for download (http://mgg.coas.oregonstate.edu/~andreas/Nitrogen/n15database.html). Figure 9 shows the annually averaged global distribution of available observations, averaged over 200 - 300 m depth to illustrate the spatial coverage. Seasonal sampling biases exist depending on the region. More details about the data sets can be found in the respective subsections below, where comparisons are presented for the Southern Ocean (Indian-Pacific sector), the Eastern Tropical North Pacific, the Central Equatorial Pacifc and the Subtropical North Atlantic. Other regions with available $\delta^{15}NO_3^-$ observations included in the dataset but not discussed in the text are the Bering Sea [*Lehmann et al.*, 2005], Northeast Pacific [*Galbraith*, 2006], and the Arabian Sea [*Altabet et al.*, 1999].

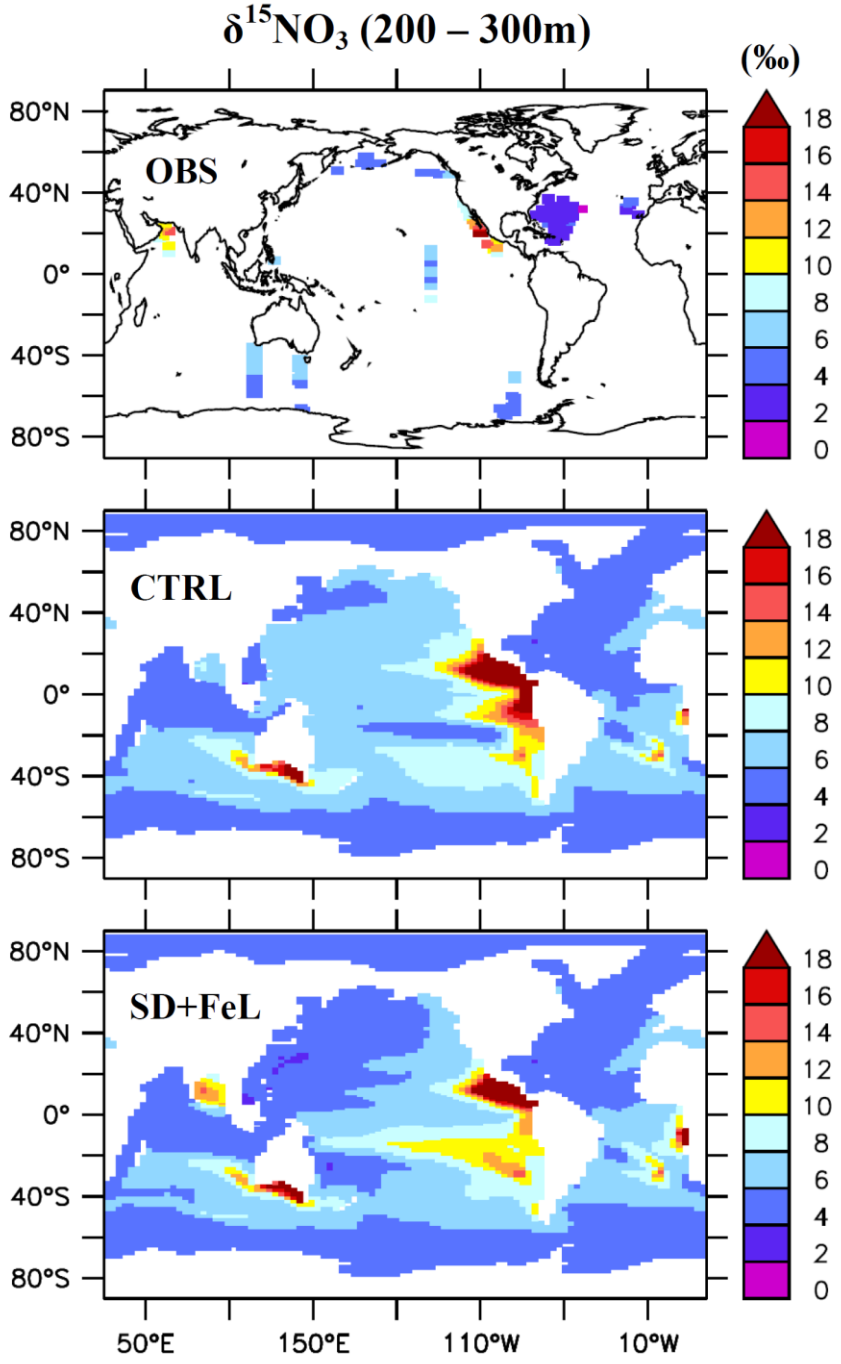

Figure 9. Comparison of annual $\delta^{15}NO_3^-$ (‰) averaged over 200 m – 300 m of available observations (OBS), CTRL, SedDeni+FeLim (SD+FeL) experiment.

4.1 Southern Indian-Pacific Ocean

The Southern Ocean represents a critical region of biogeochemical cycling in the ocean because it is the largest open ocean region with incomplete drawdown of the major nutrients. This results in an excess amount of CO_2 at the surface, which is released to the atmosphere. The degree to which surface nutrients are utilized here may have profound impacts on ocean-atmosphere exchanges of CO_2. Figure 10 shows a comparison with observations recorded in the region [*Sigman et al.*, 1999; *Altabet and Francois*, 2001; *DiFiore et al.*, 2006]. This data sub-set compiles observations from 8 cruises covering various seasons. Since all cruises do not cover the same location, some seasonal biases may occur. Nevertheless, below we show annual averages for maximum spatial coverage. The model does not capture interannual variability (due to the prescribed monthly climatological winds) of some observations but it still simulates the general inverse trend of increasing $\delta^{15}NO_3^-$ with decreasing NO_3^- (Figure 10a). However, the model underestimates the slope suggesting that the enrichment factor for NO_3^- assimilation used in the model (ε_{ASSIM} = 5‰) is too low, in agreement with *DiFiore et al.* [2006].

The biggest apparent discrepancy with the observations is the overestimation of simulated surface (0 – 130 m) $\delta^{15}NO_3^-$ north of 40°S off the southern coast of Australia (Figure 10c). This can be explained by overestimated surface NO_3^- utilization relative to observations (i.e. too low NO_3^- concentrations) in the model (Figures 6, Figure 10c-contour line). Where the simulated surface NO_3^- is almost completely depleted (i.e., $NO_3^- < 2$ μmol kg^{-1}) (see Figure 10c-contour line), the remaining $\delta^{15}NO_3^-$ becomes higher than 20‰. Since none of the existing $\delta^{15}NO_3^-$ observations were collected in such low NO_3^- concentrations (Figure 10a), it is not possible to falsify this model response at this time.

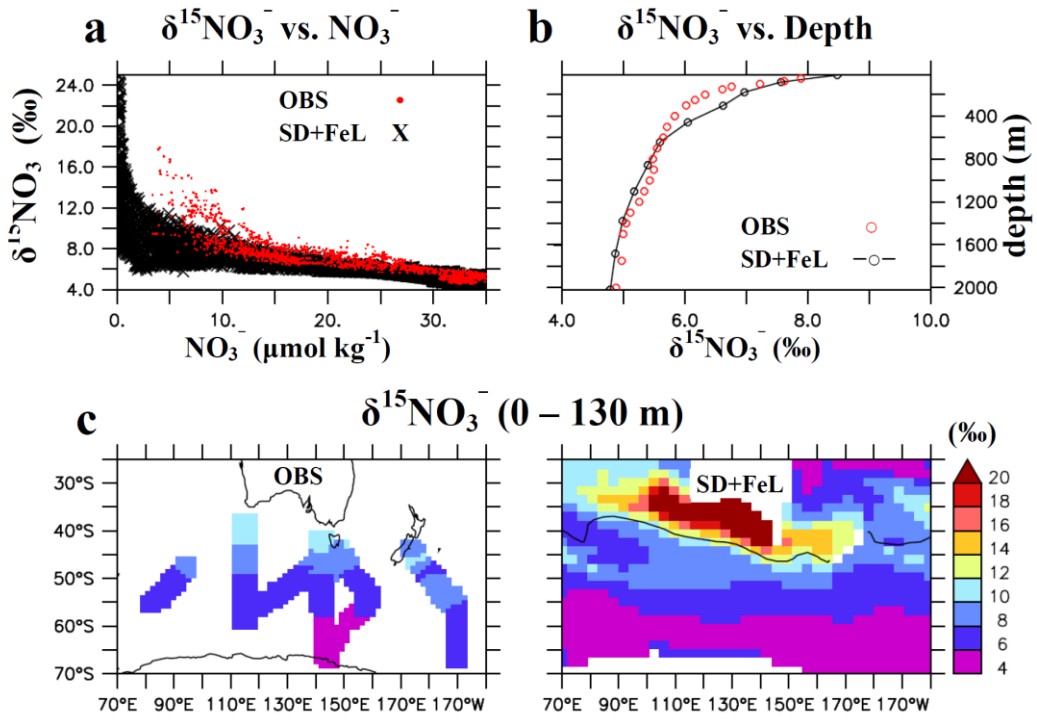

Figure 10. Comparison of the Indian-Pacific sector of the Southern Ocean with the $\delta^{15}NO_3^-$ database (OBS) and SD+FeL. (a) $\delta^{15}NO_3^-$ vs. NO_3^-; (b) horizontally averaged (over available data south of the 2 µmol kg^{-1} NO_3^- contour) depth $\delta^{15}NO_3^-$ profiles; (c) surface $\delta^{15}NO_3^-$ with a NO_3^- contour line of 2 µmol kg^{-1} (note no NO_3^- observations are below 2 µmol kg^{-1}).

4.2 Eastern Tropical North Pacific

The ETNP contains the largest suboxic zone in the ocean, where water column denitrification occurs. The relatively small spatial scale of suboxic zones makes them difficult for the model to simulate accurately and deficiencies in the coarse resolution physical circulation model prevent it from fully resolving some important physical processes, especially in coastal regions. Underestimating coastal upwelling results in corresponding underestimation of primary production, OM remineralization, and O_2 consumption at depth. This is a major reason for overestimated dissolved O_2 at depth in areas with significant coastal upwelling (e.g., off Peru and NW Mexico) (Figure 3). Preliminary experiments (not shown) suggest that increased vertical resolution can significantly improve the simulation of productivity and suboxia in the Eastern Tropical South Pacific.

The ability to reproduce the equatorial undercurrents that transport relatively oxygen-rich water from the western basin is also important in the simulation of the Eastern Pacific suboxic zones. The anisotropic viscosity scheme [*Large et al.*, 2001] improves equatorial dynamics considerably (Appendix A). The Pacific Equatorial Undercurrent increases from 0.15 m/s to nearly 0.8 m/s, just slightly weaker than observations, which show velocities near 1 m/s (Figure A2). The North Equatorial Countercurrent in the model also displays lower current velocities than observed, and does not deliver enough oxygen-rich water directly into the ETNP suboxic zone. This is likely the main reason why the simulated suboxic zone is much larger than observed towards the equator in the ETNP (Figures 6, 11).

Figure 11 shows October-November averaged model $\delta^{15}NO_3^-$ compared to observations from cruises during November 1999 [*Sigman et al.*, 2005] and October 2000 [*Altabet*, unpublished]. The model is able to capture the general observed trend of increasing $\delta^{15}NO_3^-$ as NO_3^- is consumed during water column denitrification (Figure 11a). Due to the physical circulation model's deficiencies mentioned above,

the simulated suboxic zone is too large and located too far south by ~5° compared to observations (Figure 6, Figure 11c-contour line). This results in higher rates of water column denitrification that lead to higher $\delta^{15}NO_3^-$ values and more N-deficient water in the core of the suboxic zone relative to observations. Figure 11b compares the horizontally averaged $\delta^{15}NO_3^-$ depth profiles only within the hypoxic zone (O_2 < 10 μM) at 300 m (contoured on Figure 11c) to account for the displaced OMZ. Within this region, the model is able to capture the general vertical distribution of $\delta^{15}NO_3^-$ seen in the observations such as the surface minimum and subsurface maximum.

$\delta^{15}NO_3^-$ in the ETNP decreases towards the surface [*Cline and Kaplan,* 1975; *Brandes et al.,* 1998; *Voss et al.,* 2001; *Sigman et al.,* 2005] suggesting a source of isotopically light N at the surface. *Brandes et al.* [1998] proposed that in the Arabian Sea as much as 30% of primary production must be supported by N_2 fixation in order to account for the low surface $\delta^{15}NO_3^-$. Other observations also suggest that the decrease in $\delta^{15}NO_3^-$ towards the surface is likely due to the fixation of atmospheric N_2 and the subsequent, closely coupled remineralization-nitrification cycle [*Sigman et al.,* 2005]. We test this hypothesis by comparing the observations with the model experiment in which the isotope effect of N_2 fixation is neglected ("No NFIX"). In this case, the model overestimates surface $\delta^{15}NO_3^-$ by ~10‰ (Figure 11b). The input of isotopically light fixed-N from N_2 fixation is required in the model to closely simulate the decreasing trend of $\delta^{15}NO_3^-$ towards the surface. In the model 20% of the fixed-N loss via denitrification is re-introduced into the surface by N_2 fixation occurring directly above the denitrification zone in the ETNP.

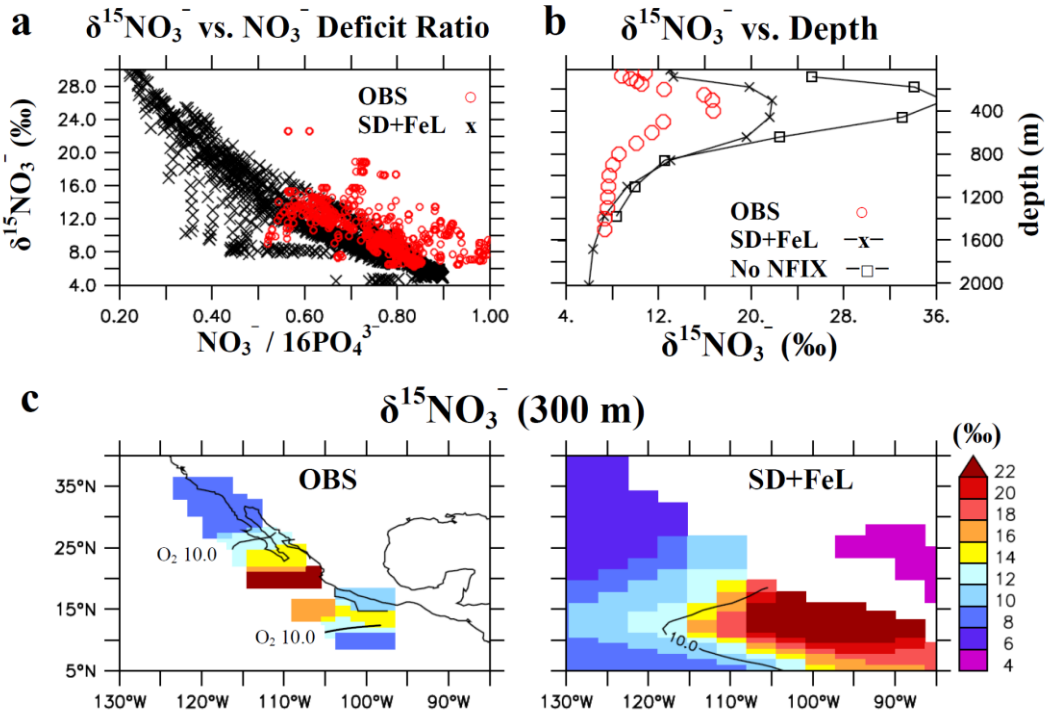

Figure 11. Comparison of the ETNP with the $\delta^{15}NO_3^-$ database and SD+FeL. (a) $\delta^{15}NO_3^-$ vs. NO_3^- Deficit Ratio; (b) horizontally averaged (within 10 µM O_2 contour) depth $\delta^{15}NO_3^-$ profiles including the experiment where the isotope effect of N_2 Fixation is neglected (No NFIX); (c) subsurface $\delta^{15}NO_3^-$ with a O_2 contour line of 10 µmol kg^{-1}.

4.3 Central Equatorial Pacific

The Central Equatorial Pacific is in close proximity to the suboxic zones in the Eastern Pacific and also has large surface NO_3^- gradients making it a useful region to test the influences of denitrification, N_2 fixation, and algal NO_3^- utilization on $\delta^{15}N$ in the model. Figure 12 compares observational $\delta^{15}N$-OM [*Altabet and Francois*, 1994] with the model simulations at 140°W. The ability to simulate $\delta^{15}N$-OM that eventually reaches the sea floor can be a powerful tool to interpret sedimentary $\delta^{15}N$ changes throughout Earth's history. $\delta^{15}N$-OM shows a decreasing northward trend in the SD+FeL experiment with a minimum at the equator. This minimum at the equator is caused by the low degree of NO_3^- utilization because of the large supply of NO_3^- to the surface via strong equatorial upwelling. The northward decreasing $\delta^{15}NO_3^-$ trend is due to more N_2 fixation occurring north of the equator, where sufficient aeolian Fe deposition exists. When this aeolian Fe limitation parameterization of diazotrophy is not included in the model (SD), the meridional $\delta^{15}N$ trend cannot be simulated, confirming that aeolian Fe deposition has an important control on the distribution of N_2 fixation across in the Pacific Ocean (Figure 12).

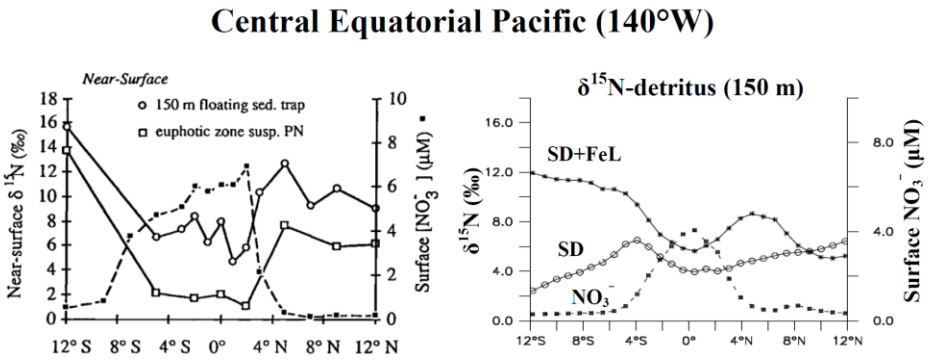

Figure 12. Comparison of δ^{15}N-detritus (‰) with observations [*Altabet and Francois*, 1994] in the Tropical Pacific Ocean at 140°W.

4.4 Western Pacific

The Western Pacific is "downstream" to the denitrification zones of the Eastern Pacific, representing a potential region where N_2 fixation may occur when low N' water flows westward out of the eastern high surface nutrient cold tongue. However, along the equator evidence does not suggest the input of isotopically light atmospheric N_2 being introduced into the system via N_2 fixation [*Yoshikawa et al.,* 2006]. This region has very low amounts of aeolian dust and Fe deposition [*Jickells et al*., 2005; *Fan et al.*, 2006], which may help inhibit N_2 fixation. If N_2 fixation does not occur here, this low N' water will need to travel someplace where enough Fe is available to support N_2 fixation (e.g., in the Atlantic or Indian Ocean).

Since the majority of continental land masses exist in the northern hemisphere, aeolian dust deposition is larger in the North Pacific than in the South Pacific (Figure 3). Thus, enough dissolved Fe in surface water may exist in the Northwest Pacific to support N_2 fixation that can restore N' to near zero and balance the fixed N budget. However, the Southern Ocean is the largest HNLC region limited by Fe. Low N' water that flows southwards may remain N-deficient until it eventually reaches other Fe sufficient water (e.g., in the Atlantic or Indian Ocean). This would imply an interbasin ocean circulation-regulated centennial to millennial timescale for balancing the fixed N loss due to denitrification by N_2 fixation.

Three data sets are compared to zonally averaged model subsurface $\delta^{15}NO_3^-$ in the Western North Pacific (Fig. 13). The observations indicate a trend of heavier $\delta^{15}NO_3^-$ near the equator to lighter values northward, suggesting more N_2 fixation occurring at higher latitudes, where aeolian dissolved Fe deposition is larger. The SD+FeL experiment generally captures this northward trend while CTRL simulates the opposite. This suggests that dissolved Fe deposition is indeed an important component in supporting growth by N_2 fixation, and may be limiting the ability of diazotrophs to compensate the fixed N loss from denitrification.

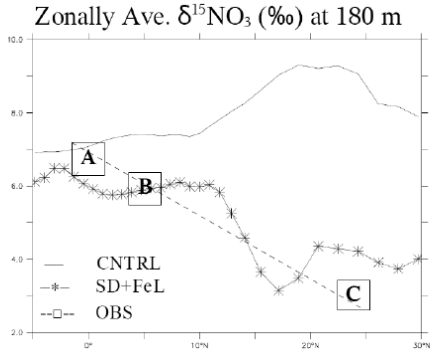

Figure 13. Western North Pacific zonally averaged model $\delta^{15}NO_3^-$ (‰) over 120°E to 150°E at 180 m depth compared with values recorded at the same depth in the region (boxes) at their respective latitude: (A) ~6.75‰ from *Yoshikawa et al.* [2006] at 0°N/S, 140°E - 150°E; (B) ~6‰ from *Kineast et al.* [2008] at 6°N, 125°E; (C) ~3 from *Liu et al.* [1995] at 25°N, 123°E.

4.5 North Atlantic

Uncertainties regarding processes that can affect the nitrogen isotope signal in the North Atlantic make it challenging to interpret and simulate nitrogen isotopes. Estimates of atmospheric N deposition [*Duce et al.*, 2008] and the assimilation-remineralization-nitrification cycle are not well constrained. Although atmospheric N deposition may be significant in this region [*Michaels et al.*, 1996; *Lipschultz et al.*, 2002; *Hansell et al.*, 2004 and 2007; *Knapp et al.*, 2005 and 2008], its isotopic composition is not well known and therefore it is not included in this model version. Figure 14 shows the comparison of annual model $\delta^{15}NO_3^-$ with available observations from cruises in May 2001, 2004 [*Altabet and Montoya*, unpublished], October 2002 [*Knapp et al.*, 2008], and May 2005 [*Bourbounnais et al.*, 2009]. The model overestimates the $\delta^{15}NO_3^-$ values everywhere, by 0.9‰ on average, presumably mostly due to the underestimation of N_2 fixation, but possibly also because of atmospheric N deposition and/or fractionation during the remineralization of organic matter are not included, both of which would act to decrease subsurface values of $\delta^{15}NO_3^-$. Underestimated N' in the North Atlantic (Figure 5) also indicate too little N_2 fixation in the model, however, we note that the too low N:P ratio of diazotrophs also contributes to this N' underestimation.

N_2 fixation is most likely underestimated because DOM dynamics are not included in the model. It has been suggested that DOP is more labile relative to DON, which can help relieve diazotrophs of P limitation in regions mainly fueled by microbial remineralization loops [*Wu et al.*, 2000], and increase N_2 fixation. However, the model still does simulate the general pattern of low $\delta^{15}NO_3^-$ in the thermocline, just not to the extent present in the observations. The amount of sedimentary denitrification that occurs in the North Atlantic is found to stimulate enough N_2 fixation to match the general $\delta^{15}NO_3^-$ trend, because when sedimentary denitrification is switched off the thermocline minimum is not simulated. This

suggests that sedimentary denitrification has an important influence of N_2 fixation in the Subtropical North Atlantic.

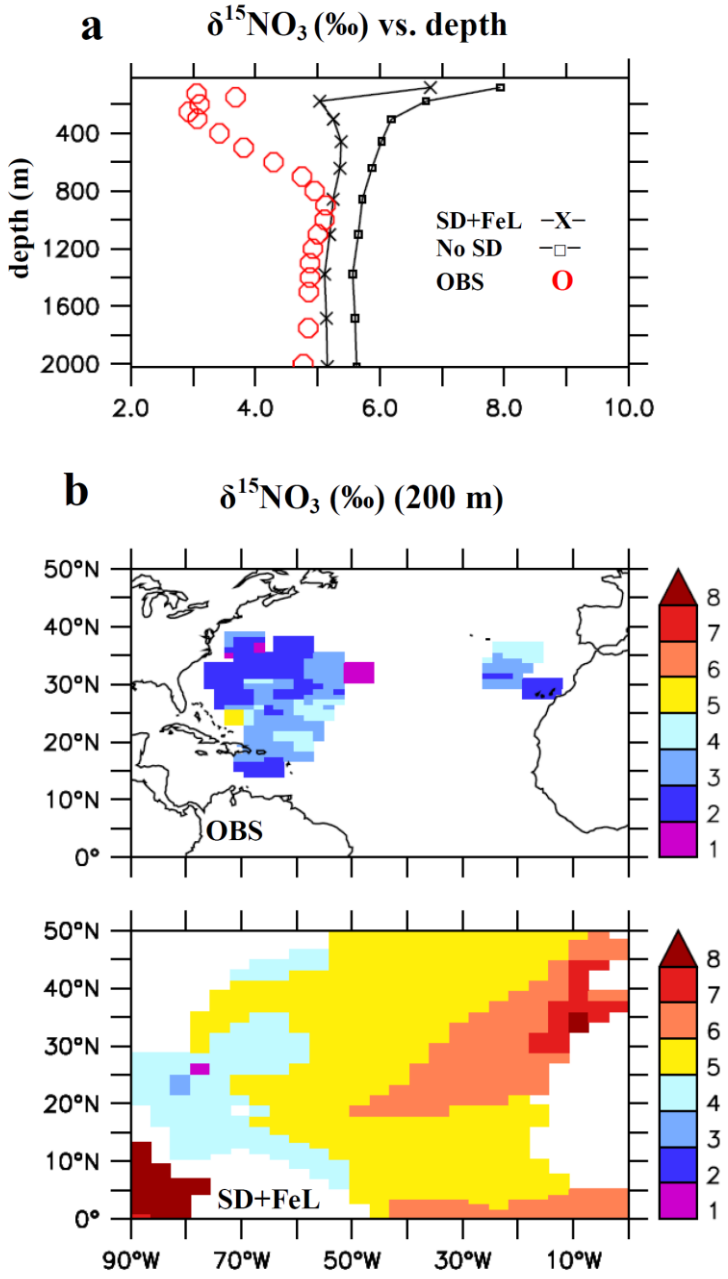

Figure 14. Comparison of the North Atlantic with the $\delta^{15}NO_3^-$ database and SD+FeL. (a) Horizontally averaged (over available data) depth $\delta^{15}NO_3^-$ profiles including the experiment where sedimentary denitrification is switched off (No SD); (b) subsurface $\delta^{15}NO_3^-$ in the database (OBS) and model (SD+FeL).

Chapter 5: Discussion

The isotope effect sensitivity experiments shown above have isolated the different spatial patterns of $\delta^{15}N$ resulting from different N-transformational processes. These simulations show that the isotope effect of algal NO_3^- assimilation can drive very large spatial gradients in both $\delta^{15}NO_3^-$ and $\delta^{15}N$-OM (Figure 7). While this isotope effect increases $\delta^{15}NO_3^-$ everywhere, the change in $\delta^{15}N$-OM depends on the ocean environment. In HNLC areas where surface NO_3^- utilization is low and algae are able to fractionate NO_3^- near their designated value during assimilation, the resulting $\delta^{15}N$-OM value decreases. However when NO_3^- utilization is high, the $\delta^{15}N$-OM value is more similar to the $\delta^{15}NO_3^-$ value it consumes because the effective degree of fractionation becomes much lower and the conservation of isotope mass balance (See Section 3). This suggests that changes in the extent of HNLC regions, for example due to changes in ocean circulation or aeolian dust deposition, can drive large changes in $\delta^{15}NO_3^-$ and $\delta^{15}N$-OM. The strong influence of surface NO_3^- utilization effect on the distribution of N isotopes in the model suggests that changes in surface NO_3^- utilization patterns throughout Earth's history could have contributed to large fluctuations in $\delta^{15}N$ observed in sediment records, especially near fronts where large surface NO_3^- gradients exist (See also *Altabet and Francois* [1994]*; Farrell et al.* [1995]; *Francois et al.* [1997]; *Sigman et al.* [1999]; *Robinson et al.* [2005]; *Brunelle et al.* [2007]; *Galbraith et al.* [2008]).

The model simulates a strong direct and indirect isotope effect of denitrification. High $\delta^{15}NO_3^-$ produced by water column denitrification has clear regional impacts and is also responsible to overall elevated $\delta^{15}NO_3^-$ for the ocean relative to the N_2 fixation source (See below). The indirect effect of both water column and sediment denitrification includes creation of N-deficient water, which creates an ecological niche for diazotrophs. This stimulates additional N_2 fixation when other suitable conditions for N_2 fixation exist (e.g., warm (> 20°C), N-depleted

surface water with sufficient Fe and P). This indirect effect also attenuates the horizontal circulation of high $\delta^{15}NO_3^-$ waters, originating from regions of water column denitrification, because N_2 fixation introduces much lower $\delta^{15}N$ into the ocean, which causes the direct isotope effect of water column denitrification to be regionalized to suboxic zones in the model.

In the model, N_2 fixation in basins with high production over continental shelves, such as the North Atlantic, is significantly stimulated by sedimentary denitrification to create a subsurface $\delta^{15}NO_3^-$ minimum, which is in better agreement with observations. Thus, N_2 fixation in the ocean may be affected by the area of continental shelves (where the majority of the global sedimentary denitrification occurs), which in turn is a function of global sea level [*Christensen et al.*, 1987; *Altabet and Curry*, 1989]. This suggests that glacial/interglacial changes in N_2 fixation in the subtropical North Atlantic may have partly been driven by sea level change (See also *Ren et al.*, [2009]).

The qualitative and quantitative agreement with the nitrogen isotope observations suggests that the model captures some of the essential nitrogen cycle dynamics of the real ocean. A direct coupling between denitrification and N_2 fixation occurs in the ETNP where suboxic subsurface waters are directly overlain by N-depleted surface waters. This is an environment where diazotrophs can thrive, add to the OM export production, and, upon sinking and remineralization at depth, help maintain suboxic O_2 levels. Thus, a local positive feedback is created. The sharp decrease in $\delta^{15}NO_3^-$ from the subsurface suboxic zone towards the surface in the ETNP (Figure 11b) can best be explained by the direct coupling of N_2 fixation and denitrification in the model. N_2 fixation accounts for 20% of the fixed-N lost via water column denitrification in the ETNP, indicating that N_2 fixation is able to partially balance fixed N loss via water column denitrification, at least if surface waters above the denitrifying zones are depleted of N. Our estimated for the N-loss

compensation by N_2 fixation is lower than previous estimates (e.g., 30% [*Brandes et al.*, 1998] and 65% [*Sigman et al.*, 2005]), but we note a better simulation of the suboxic zone is needed for a more reliable estimate.

Our results also show the importance denitrification has on the global budget of nitrogen isotopes. N_2 fixation and total denitrification become balanced as the model approaches equilibrium, and the ratio of fixed-N loss, which is fractionated (water column denitrification) to fixed-N loss without fractionation (sedimentary denitrification), will set the global oceanic average $\delta^{15}NO_3^-$. Note that, since the majority of sedimentary denitrification occurs on the coastal shelves that are not well resolved in the model, sedimentary denitrification is tuned so the simulated deep ocean $\delta^{15}NO_3^-$ is near the observed value of 5‰. The ratio of sedimentary denitrification to water column denitrification in the model is 1.3:1, but is very sensitive to the isotope effect of water column denitrification [*Altabet*, 2007].

Because the model exaggerates the dimension of the suboxic zone, subsurface NO_3^- consumption by denitrifying bacteria in the Eastern Pacific is overestimated (Figures 6, 11). This water obtains a very high $\delta^{15}NO_3^-$ signature, but when it mixes with higher NO_3^- (and lower $\delta^{15}NO_3^-$) water just outside the water column denitrification zone, the high $\delta^{15}NO_3^-$ signature becomes largely averaged out of the resulting mean $\delta^{15}NO_3^-$ value because $\delta^{15}NO_3^-$ is weighted towards the water parcel with higher NO_3^-. This "dilution effect" reduces the effective N isotope effect for N-elimination significantly (See also *Deutsch et al.* [2004]). This dilution effect also partly explains why our relatively low water column to sedimentary denitrification ratio significantly differs from estimates based on a one-box model by *Brandes and Devol* [2002], which yielded a ratio of ~4:1. However, *Brandes and Devol* [2002] assumed a constant N isotope effect of ~25%, not considering that NO_3^- is being denitrified from a partially depleted heterogeneous N pool, so that the effective N isotope effect of water column denitrification in their model is likely overexpressed.

Our estimate is in better agreement with the box model of *Altabet* [2007], which again does not consider heterogeneous NO_3^- pools, but does account for a NO_3^- consumption effect, which reduces the effective fractionation of water column denitrification as NO_3^- is consumed, and also suggests a ratio near 1:1. Both the dilution and NO_3^- consumption effect contribute to the relatively low ratio predicted by our model. However, more realistic simulations of all suboxic zones are needed for more reliable estimates. Our study emphasizes the importance of understanding the combined effective N isotope effects of water column denitrification and sedimentary denitrification.

With regards to the large scale denitrification-N_2 fixation feeback, the SD+FeL experiment is in general agreement with the model of *Moore and Doney*, [2007], which dynamically include Fe in their model. The qualitative denitrification-N_2 fixation coupling was similar to that observed in our simulations. In both cases, the Pacific Ocean is a sink of fixed nitrogen because of a weak coupling between N_2 fixation and denitrification, whereas the Atlantic and Indian Oceans are a sources of fixed N as low N' waters circulate out of the Pacific into these basins, allowing more N_2 fixation to occur there. As *Moore and Doney* [2007] noted, this pattern of N_2 fixation differs from that in the model of *Deutsch et al.*, [2007], which simulates a tighter coupling in the Eastern Pacific which is more similar to our CTRL simulaiton. *Deutsch et al.* [2007]'s highest N_2 fixation rates occur in the equatorial cold tongue upwelling regime in waters with high NO_3^- concentrations, which may seem implausible given that the diazotroph *Trichodesmium* can more efficiently assimilate NO_3^- than molecular N_2 during photosynthesis if it is available [*Holl and Montoya*, 2005]. Diazotrophs have this ability in our model which is why N_2 fixation is not simulated there.

A potential centennial to millennial timescale delay of N_2 fixation to changes in denitrification may represent a long enough period of time to significantly perturb

the global oceanic fixed N inventory. A major change in the oceanic N pool can impact the strength of the biological pump and, in turn, atmospheric CO_2 concentrations. Sedimentary nitrogen isotope records in the Eastern North Pacific, which have been interpreted as changes in water column denitrification, show large increases during the last glacial-interglacial transition [*Ganeshram et al*., 1995 and 2000; *Emmer and Thunell*, 2000; *Kineast et al.*, 2002; *Hendy et al.*, 2004]. If water column denitrification did actually increase over this period, it would suggest that the oceanic fixed N inventory could have remained in deficit for a long time. We speculate that a phase of global fixed N deficiency might have contributed to rising atmospheric CO_2 concentrations during the deglaciation.

Chapter 6: Conclusions

A new model of nitrogen isotopes has been implemented into the three-dimensional ocean component of a global Earth System Climate Model capable of millennial timescale simulations. Despite some model deficiencies, we have shown that this model can successfully reproduce the general spatial patterns of observational $\delta^{15}NO_3^-$. Sensitivity experiments allowed us to isolate the individual effects of different N-transformational processes on the global distribution of $\delta^{15}N$. Algal NO_3^- assimilation, N_2 fixation and water column denitrification are all similarly important in setting the global patterns of nitrogen isotope ratios in the ocean, whereas the effect of zooplankton excretion is smaller. Both water column and sedimentary denitrification also have important indirect effects on the nitrogen isotopes distribution by creating N-deficient water, which stimulates additional N_2 fixation.

Key features of the model have been identified that are in need of further development. The coarse resolution physical circulation model does not fully resolve the dynamics of coastal upwelling regimes, which in part drive the flux of OM towards the sea floor sediments and its remineralization in the water column, as well as indirectly influences ventilation of suboxic zones. This is critical in the simulation of water column denitrification and sedimentary denitrification, which are important processes with respect to the global N isotope balance. Future model versions will include additional vertical levels to better resolve continental shelves, which should considerably improve the simulation of coastal dynamics.

The fast recycling microbial loop, which accounts for the recycling of organic matter into inorganic macronutrients (NO_3^-, PO_3^{3-}), is currently included as one parameterization using fixed elemental ratios (N:P = 16:1). It bypasses the need to include DOM and ammonium as variables in the model, which saves computational costs. However, it neglects some essential dynamics such as the more efficient recycling of DOP compared to DON [*Wu et al.*, 2008]. This mechanism can help

relieve diazotrophs of their P limitation and allow them to fix additional N_2 into the oceanic fixed-N pool in oligotrophic waters. The addition of dynamic elemental stoichiometry for the marine ecosystem, as well as a parameterization for the microbial loop including DOM dynamics should account for this model deficiency. The ecosystem model also suffers from the exclusion of Fe as a prognostic tracer. This prevents the model from having the capability to simulate differences in ecosystems limited by marconutrients (NO_3^-, PO_3^{3-}) versus micronutrients (Fe).

Future applications of this model will include simulations of past climates, and direct comparison with $\delta^{15}N$ sediment records will be used to test the hypotheses. The model can be a useful tool to quantify past interactions between the marine nitrogen cycle and its isotopes, as well as their impact on climate providing new insights into important physical and biogeochemical changes throughout Earth's history.

Chapter 7: Bibliography

Altabet, M. A., W. G. Deuser, S. Honjo, C. Stienen (1991), Seasonal and depth-related changes in the source of sinking particles in the North Atlantic, *Nature, 354*, 136-139

Altabet , M. A. and R. Francois (1994), Sedimentary nitrogen isotopic ratio as a recorder for surface ocean nitrate utiliztion, G*lobal Biogeochem. Cycles, 8*, 103-116

Altabet, M. A., C. Pilskaln, R. Thunell, C. Pride, C. Sigman, F. Chavez, R. Francois (1999), The nitrogen isotope biogeochemistry of sinking particles from the margin of the Eastern North Pacific, *Deep-Sea Res. I., 46*, 655-679

Altabet, M. A., D. W. Murray and W. L. Prell (1999), Climate-linked variations in Arabian Sea denitrification over the last 1 m.y.: Implications for the marine N cycle, *Paleoceanogr., 14*, 732-743

Altabet, M. A., and R. Francois (2001), Nitrogen isotope biogeochemistry of the Antarctic Polar Frontal Zone at 170W, *Deep Sea Res. II., 48*, 4247-4273

Altabet, M. A. (2001), Nitrogen isotopic evidence for micronutrient control of fractional NO_3 utilization in the equatorial Pacific, *Limnol. Oceanogr., 46*(2), 368-380

Altabet, M. A. (2005), Isotopic tracers of the marine nitrogen cycle, In: *Marine Organic Matter: Chemical and Biological Markers* edited by J. Volkman, vol. 2 of "The Handbook of Environmental Chemistry", Editor-in-Chief: O. Hutzinger, pp. 251-293, http://dx.doi.org/10.1007/698_2_008

Altabet, M. A., Higginson, M., and Murray, D. W. (2007), The effect of millennial-scale changes in Arabian Sea denitrification on atmospheric CO_2, *Nature, 415*, 159-162

Altabet, M. A. (2007), Constraints on oceanic N balance/imbalance from sedimentary ^{15}N records, *Biogeosciences, 4*, 75-86

Berelson, W. M. (2002), Particle settling rates increase with depth in the ocean, *Deep-Sea Res., 49*, 237-251

Bourbonnais, A., M. F. Lehmann, J. J. Waniek, and D. E. Schulz-Bull (2009), Nitrate isotope anomalies reflect N_2 fixation in the Azores Front region (subtropical NE Atlantic), *Journal of Geophys. Res., 114*, CO3003, doi:10.1029/2007JC004617

Brandes, J. A., and A. H. Devol (1997), Isotopic fractionation of oxygen and nitrogen in coastal marine sediments, *Geochim. et Sosmo. Acta*, *61*(9), 1793-1801

Brandes, J. A., A. H. Devol, T. Yoshinari, D. A. Jayakumar, S. W. A. Naqvi (1998), Isotopic composition of nitrate in the central Arabian sea and eastern tropical pacific: A tracer of mixing and nitrogen cycles, *Limnol. Oceanogr.*, *43*(7), 1680-1689

Brandes, J. A, and A. H. Devol (2002), A global marine-fixed nitrogen isotopic budget: Implications for Holocene nitrogen cycling, *Global Biogeochem. Cycles*, *16*, 1120, doi:10.1029/2001GB001856

Brunelle, B. G., D. M. Sigman, M. S. Cook, L. D. Keigwin, g. H. Haug, B. Plessen, B. Schettler, S. L. Jaccard (2007), Evidence from diatom-bound nitrogen isotopes for subarctic Pacific stratification during the last ice age and a link to North Pacific denitrification changes, *Paleoceangr.*, *22*, PA1215, doi:10.1029/2005PA001205

Bryan, K., S. Manabe, R. C. Pacanowski (1975), A global ocean-atmosphere climate model. Part II: The ocean circulation, *J. Phys. Oceanogr.*, *5*, 30-46

Capone, D. G., J. P. Zehr, H. Paerl, B. Bergman, and E. J. Carpenter (1997), *Trichodesmium*, a globally significant marine cyanobacterium, *Science*, *276*, 1221-1229

Carpenter, D. G., H. R. Harvey, B. Fry, D. G. Capone (1997), Biogeochemical tracers of the marine cyanobacterium *Trichodesmium*, *Deep-Sea Res. I*, *44*, 27-38

Checkley, Jr., D. M. and C. A. Miller (1989), Nitrogen isotope fractionation by oceanic zooplankton, *Deep Sea Res.*, *36*, 1449-1456

Cline, J. D. and I. R. Kaplan (1975), Isotopic fractionation of dissolved nitrate during denitrification in the eastern tropical North Pacific Ocean, *Mar. Chem.*, *3*, 271-299

Codispoti, L. A., and F. A. Richards (1976), An analysis of the horizontal regime of denitrification in the eastern tropical North Pacific, *Limnol. Oceanogr.*, *21(3)*, 379-388

Codispoti, L. A. (2007), An oceanic fixed nitrogen sink exceeding 400 Tg N a^{-1} vs the concept of homeostasis in the fixed-nitrogen inventory, *Biogeosciences*, *4*, 233-253

De Pol-Holz, R., O. Ulloa, L. Dezileau, J. Kaiser, F. Lamy, D. Hebbeln (2006), Melting of the Patagonian Ice Sheet and deglacial perturbations of the nitrogen

cycle in the eastern South Pacific, *Geophy. Res. Lett.*, *33*, L04704, doi:10.1029/2005GL024477

Delaney, M. L. (1998), Phosphorus accumulation in marine sediments and the oceanic phosphorus cycle, *Blobal Biogeochem. Cycles*, *12*(4), 563-572

Deutsch, C., D. M. Sigman, R. C. Thunell, A. N. Meckler, G. H. Haug (2004), Isotopic constraints on glacial/interglacial changes in the oceanic nitrogen budget, *Global Biogeochem. Cycles*, *18*, GB4012, doi:10.1029/2003GB002189

Deutsch, C., J. L. Sarmiento, D. M. Sigman, N. Gruber, J. P. Dunne (2007), Spatial coupling of nitrogen inputs and losses in the ocean, *Nature*, *445*, doi:10.1038/nature05392

Delwiche, C. C. and P. L. Steyn (1970), Nitrogen isotope fractionation in soils and microbial reactions, *Envrion. Sci. Technol.*, *4*, 929-935

DiFiore, P. J., D. M. Sigman, T. W. Trull, M. J. Lourey, K. Karsh, G. Cane, R. Ho (2006), Nitrogen isotope constraints on subantarctic biogeochemistry, *J. Geophys. Res.*, *111*, C08016, doi:10.1029/2005JC003216

Emmer, E., and R. C. Thunell (2000), Nitrogen isotope variations in Santa Barbara Basin sediments: Implications for denitrification in the eastern tropical North Pacific during the last 50,000 years, *Paleoceanograhy*, *15*, 377-387

Falkowski, P. G. (1997), Evolution of the nitrogen cycle and its influence on the biological sequestration of CO_2 in the ocean, *Nature*, *387*, 272-275

Fan, S.-M., W. J. Moxim, H. L. Il (2006), Aeolian input of bioavailable iron to the ocean, *Geophys. Res. Letters, 33*, L07602, doi:10.1029/2005GL024852

Farrell, J. W., T. F. Pedersen, S. E. Calvert, B. Nielsen (1995), Glacial-interglacial changes in nutrient utilization in the equatorial Pacific Ocean, *Nature*, *377*, 514-517

Fogel, M. L., and L. A. Cifuentes (1993), Isotope Fractionation during Primary Production. In: Engel, M.H. and A. Macko (Editors), *Organic Geochemistry*, Plenum Press, New York, pp. 861

Francois, R., M. A. Altabet, E-F. Yu, D. M. Sigman, M. P. Bacon, M. Frank, G. Bohrmann, G. Barelle, L. D. Labeyrie (1997), Contribution of southern ocean surface-water stratification to low atmospheric CO2 concentrations during the last glacial period, *Nature*, *389*, 929-936

Galbraith, E (2006), Interactions between climate and the marine nitrogen cycle on glacial-interglacial time scales, Ph.D. thesis, University of British Columbia

Ganeshram, R. S., T. F. Pedersen, S. E. Calvert, J. W. Murray (1995), Large changes in oceanic nutrient inventories from glacial to interglacial periods, *Nature*, *376*, 755-758

Ganeshram, R. S., T. F. Pedersen, S. E. Calvert, G. W. McNeill, M. R. Fontugne (2000), Glacial-interglaical variability in denitrification in the World's Oceans: Causes and consequences, *Paleoceanogr.*, *15*, 361-376

Gaye-Haake, B., N. Lahajnar, L.-Ch. Emeis, D. Unger, T. Rixen, A. Suthhof, V. Ramaswamy, H. Schulz, A. L. Paropkari, M. V. S. Guptha, V. Ittekkot, (2005), Stable nitrogen isotope ratios of sinking particles and sediments from the nothern Indian Ocean, *Mar. Chem.*, *96*(3-4), 243-255, doi:10.1016/j.marchem.2006.02.001

Gent, P. R., and J. C. McWilliams (1990), Isopycnal mixing in ocean circulation models, *J. Phys. Oceanogr.*, *20*, 150-155

Giraud, X., P. Bertrand, V. Garcon, I. Dadou (2000), Modeling δ15N evolution: First palaeoceanographic applications in a coastal upwelling system, *J. Mar. Res.*, *58*, 609-630

Grantham, B. A., F. Chan, K. J. Nielsen, D. S. Fox, J. A. Barth, A. Huyer, J. Lubchenco and B. A. Menge (2004), Nearshore upwelling-driven hypoxia signals ecosystem and oceanographic changes in the NE Pacific, *Nature*, *429*, 749-754

Gruber, N. and J. L. Sarmiento (1997), Global patterns of marine nitrogen fixation and denitrification, *Global Biogeochem. Cycles*, *11*, 235-266

Hansell, D. A., N. R. Bates (2004), Excess nitrate and nitrogen fixation in the North Atlantic, *Marine Chemistry*, *84*, 243-265

Hansell, D. A., D. B. Olson, F. Dentener, L.M. Zamora (2007), Assessment of excess nitrate development in the subtropical North Atlantic, *Marine Chem.*, *106*, 562-579

Hendy, I. L., T. F. Pedersen, J. P. Kennett, R. Tada (2004), Intermittent existence of a southern Californian upwelling cell during submillennial climate change of the last 60 kyr, *Paleoceanography*, *19*, PA3007, doi:10.1029/2003PA000965

Holl, C. M. and J. P. Montoya (2005), Interactions between nitrate uptake and nitrogen fixation in continuous cultures of the marine diazotroph *Trichodesmium* (cyanobacteria), *J. Phycol.*, *41*(6), 1178-1183

Jickells, T. D., Z. S. An, K. K. Andersen, A. R. Baker, G. Bergametti, N. Brooks, J. J. Cao, P. W. Boyd, R. A. Duce, K. A. Hunter, H. Kawahata, N. Kubilay, J. laroche, P. S. Liss, N. Mahowald, J. M. Prospero, A. J. Ridgwell, I. Tegen, R. Torres (2005), Global Iron Connections Between Desert Dust, Ocean Biogeochemistry, and Climate, *Science*, *308*, 67-

Karl, D, A. Michaels, B. Bergman, D. Capone, E. Carpenter, R. Letelier, F. Lipschultz, H. Paerl, D. Sigman, L. Stal (2002), Dinitrogen fixation in the world's oceans, *Biogeochemistry*, *57/58*, 47-98

Kessler, W. S. (2006), The circulation of the eastern tropical Pacific: A review, *Progress in Oceanogr.*, *69*, 181-217

Kineast, S. S., S. W. Calvert, T. F. Pedersen (2002), Nitrogen isotope and productivity variations along the northeast Pacific margin over the last 120 kyr: surface and subsurface paleoceanography, *Paleoceanogr.*, *17*(4), 1055, doi:10.1029/2001PA000650

Knapp, A. N., D. M. Sigman, F. Lipschultz (2005), N isotopic composition of dissolved organic and nitrate at the Bermuda Atlantic Time-series Study site, *Global Biogeochem. Cycles*, *19*, doi:10.1029/2004GB002320

Knapp, A. N., P. J. DiFiore, C. Deutch, D.M. Sigman, F. Lipschultz (2008), Nitrate isotopic composition for N2 fixation in the Atlantic Ocean, *Global Biogeochem. Cycles*, *22*, GB3014, doi:10.1029/2007GB003107

Kustka, A., E. J. Carpenter, and S. A. Sanudo-Wilhelmy (2002), Iron and marine nitrogen fixation: Progress and future direction, *Res. Microbiol.*, *153*, 255-262

Kuypers, M. M. M., G. Lavik, D. Woebken, M. Schmid, B. M. Fuchs, R. Amann, B. B. Jorgensen, M. S. M. Jetten (2005), Massive nitrogen loss from the Benguela upwelling system through anaerobic ammonium oxidation, *Proc. Nat. Aca. Sci.*, *102*, 5478-5483

Kuypers, M. M. M., G. Lavik, B. Thamdrup (2006) Anaerobic ammonium oxidation in the marine environment in: *Past and Present Water Column Anoxia*. *NATO Science Series*, IV. *Earth and Environmental Sciences*, *64*, edited by: L. Neretin, Springer, Dordrecht, 311-355

Large, W. C., G. Danabasoglu, J. C. McWilliams, P. R. Gent, F. O. Bryan (2001), Equatorial circulation of a global ocean climate model with anisotropic horizontal visosity, *J. Phys. Oceanogr.*, *31*, 518-536

Lehmann, M. F., S. M. Bernasconi, A. Barbieri, J. A. McKenzie (2002), Preservation of organic matter and alteration of its carbon and nitrogen isotope composition during simulated and in situ early sedimentary diagenesis, *Geochim. Cosmochim. Acta*, *66*(20), 3573-3584, doi:10.1016/S0016-7037(02)00968-7

Lehmann, M. F., D. M. Sigman, D. C. McCorkle, B. G. Brunelle, S. Hoffmann, M. Kienast, G. Cane, J. Clement (2005), Origin of the deep Bering Sea nitrate deficit: Constraints from the nitrogen and oxygen isotopic composition of water column nitrate and benthic nitrate fluxes, *Global Biogeochem. Cycles*, *19*, GB4005, doi:10.1029/2005GB0002508

Lehmann M. F., D.M. Sigman, D.C. McCorkle, J. Granger, S. Hoffmann, G. Cane, B.G. Brunelle, 2007. The distribution of nitrate 15N/14N in marine sediments and the impact of benthic nitrogen loss on the isotopic composition of oceanic nitrate, *Geochimica et Cosmochimica Acta*, doi:10.1016/j.gca.2007.07.025

Lipschultz, F., N. R. Bates, C. A. Carlson, D. A. Hansell (2002), New production in the Sargasso Sea: History and current status, *global Biogeochem. Cycles*, *16*(1), 1001, doi:10.1029/2000GB001319

Liu, K. K., and I. R. Kaplan (1989), the eastern tropical Pacific as a source of N-15 enriched nitrate in seawater off southern California, *Limnol. Oceanogr.*, *34(5)*, 820-830

Luo, C., N. Mahowald, and J. del Corral (2003), Sensitivity study of meteorological parameters on mineral aerosol mobilization, transport and distribution, *J. Geophys. Res.*, *108*(D15), 4447, doi:10.1029/2003JD003483

Macko, S. A. M. L. Fogel, P. E. Hare, and T. C. Hoering (1987), Isotope fractionation of nitrogen and carbon in the synthesis of amino acids by microorganisms, *Chem. Geol.*, *65*, 79-92

Mariotti, A., J. C. Germon, P. Hubert, P. Kaiser, R. Letolle, A. Tardieux, P. Tardieux (1981), Experimental determination of nitrogen kinetic isotope fractionation: some principles; illustration for the denitrification and nitrification processes, *Plant and Soil Science*, *62*, 413-430

Marland, G., T. A. Boden, and R. J. Andres (2006), In Trends: A Compendium of Data on Global Change, Carbon Dioxide Information Analysis Center, Oak ridge National Laboratory, U.S. Department of Energy, Oak Ridge, Tenn. USA

Matsumoto, K. et al. (2004), Evaluation of ocean carbon cycle models with data-based metrics, *Geophys. Res. Lett., 31*, L07303

McElroy, M.B. (1983), Marine biological controls on atmospheric CO_2 and climate, *Nature, 302*, 328-329

Michaels, A. F., D. Olson, J. L. Sarmiento, J. W. Ammerman, K. Fanning, R. Jahnke, A. H. Knapp, F. Lipschultz, J. M. Prospero (1996), Inputs losses and transformations of nitrogen and phosphorus in the pelagic North Atlantic, In: Howarth, R. W. (Ed.), Nitrogen Cycling in the North Atlantic Ocean and its Watersheds. Kluwer Academic Publishers, Boston, MA, pp. 181-226

Minagawa, M. and E. Wada (1984), Stepwise enrichment of 15N along food chains: Further evidence and the relation between δ15N and animal age, *Geochimica et Cosmochimica Acta, 48*, 1135-1140

Minagawa, M., and E. Wada (1986), Nitrogen isotope ratios of red tide organisms in the East China Sea - a characterization of biological nitrogen fixation, *Mar. Chem., 19(3)*, 245-259

Monnin, E., A. Indermuhle, A. Dallenbach, J. Fluckiger, B. Stauffer, T. F. Stocker, D. Raynaud, J.-M. Barnola (2001), Atmospheric CO_2 Concentrations over the Last Glacial Termination, *Science, 291*, 112-114

Montoya, J. P. and J. J. McCarthy (1995), Isotopic fractionation during nitrate uptake by phytoplankton grown in continuos culture, *J. of Plankton Res., 17*(3), 439-464

Montoya, J. P., E. J. Carpenter, D. G. Capone (2002), Nitrogen fixation and nitrogen isotope abundances in zooplankton of the oligotrophic North Atlantic, *Limnol. Oceanogr., 47*, 1617-1628

Moore, J. K. and S. C. Doney (2007), Iron availability limits the ocean nitrogen inventory stabilizing feedbacks between marine denitrification and nitrogen fixation, *Global Biogeochem. Cycles, 21*, GB2001, doi:10.1029/2006GB002762

Munk, W. H. (1950), On the wind driven ocean circulation, *J. Meteor., 7*, 79-93

Naqvi, S. S. A. (2007), The Indian Ocean, in: Nitrogen in the the Marine Environment, edited by: Capone, D. G., Bronk, D. A., Mulhollnad, M. R., and Carpenter, E. J., *Academic Press*

Postgate, J. (1998), Nitrogen Fixation 3rd edn 1-120 (Cambridge Univ. Press, Cambridge, 1998)

Raven, J. A., M. C. W. Evans, R. E. Korb (1999), The role of trace metals in photosynthetic electron transport in O_2-evolving organisms, *Photosynth. Res.*, *60*, 111-149

Ren, H., D. M. Sigman, A. N. Meckler, B. Plessen, R. S. Robinson, Y. Rosenthal, G. H. Haug (2009), Foraminiferal Isotope Evidence of Reduced Nitrogen Fixation in the Ice Age Atlantic Ocean, *Science*, *323*, 244-248

Robinson, R. S., D. M. Sigman, P. J. DiFiore, M. M. Rohde, T. A. Mashiotta, D. W. Lea (2005), Diatom-bound 15N/14N: New support for enhanced nutrient consumption in the ice age subantartctic, *Paleoceanogr.*, *20*, PA3003, doi:10.1039/2004PA001114

Sanudo-Wilhelmy, S. A., A. B. Kustka, C. J. Gobler (2001), Phosphorus limitation by *Trichodesmium* in the central Atlantic Ocean, *Nature*, *411*, 66-69

Sanudo-Wilhelmy, S. A., A. Tovar-Sanchez, F.-X. Fu, D. G. Capone, E. J. Carpenter, and D. A. Hutchins (2004), The impact of surface-adsorbed phosphorus on phytoplankton Redfield stoichiometry, *Nature*, *432*, 897-901

Schartau, M., and Oschlies, A. (2003), Simultaneous data-based optimization of a 1D-ecosystem model at three locations in the North Atlantic: Part I-Method and parameter estimates, *J. Mar. Res.*, *61*, 765-793

Schmittner, A., E. D. Galbraith, S. W. Hostetler, T. F. Pedersen, R. Zhang (2007), Large fluctuations of dissolved oxygne in the Indian and Pacific oceans during Dansgaard-Oeschger oscillations caused by variations of North Atlantic Deep Water subduction, *Paleoceangr.*, *22*, doi:10.1029/2006PA001384

Schmittner, A., A. Oschlies, H. D. Matthews, and E. D. Galbraith (2008), Future changes in climate, ocean circulation, ecosystems and biogeochemical cycling simulated for a business-as-usual CO2 emission scenario until year 4000 AD, *Global Biogeochem. Cycles*, *22*, GB1013, doi:10.1029/2007GB002953

Sigman, D. M., M. A. Altabet, R. Michener, D. D. McCorkle, B. Fry, R. M. Holmes (19997), Natural abundance-level measurement of the nitrogen isotopic compositionof oceanic nitrate: Ann adaptation of the ammonia diffusion method, *Mar. Chem.*, *57*, 227-242

Sigman, D. M., M. A. Altabet, D. D. McCorkle, R. Francois, G. Fischer (1999), The δ15N of nitrate in the Southern Ocean: Consumption of nitrate in surface waters, *Global Biogeochem. Cycles*, *13*(4), 1149-1166

Sigman, D. M., R. Robinson, A. N. Knapp, A. van Geen, D. C. McCorkle, J. A. Brandes, R. C. Thunell (2003), Distinguishing between water column and sedimentary denitrification in the Santa Barbara Basin usinkg the stable isotopes of nitrate, *Geochem., Geophys., Geosys.*, *4*(5), 1-20, doi:10.1039/2002GC00384

Sigman, D. M., J. Granger, P. J. DiFiore, M. M. Lehmann, R. Ho, G. Cane, A. van Green (2005), Coupled nitrogen and oxygen isotope measurements of nitrate along the eastern North Pacific margin, *Global Biogeochem. Cycles*, *19*, GB4022, doi:10.1029/2005GB0002458

Simmons, H. L., S. R. Jayne, L. C. St. Laurent, A. J. Weaver (2004), tidally driven mixing in a numerical model of the ocean general circulation, *Ocean Model.*, *6*, 245-263

Sutka, R. L., N. E. Ostrom, P. H. Ostrom, M. S. Phankumar (2004), Stable nitrogen isotope dynamics of idssolved nitrate in a transect from the North Pacific Subtropical Gyre to the Eastern Tropical North Pacific, *Geochimica et Cosmochimica Acta*, *68*(3), 517-527

Thamdrup, B., T. Dalsgaard, M. M. Jensen, O. Ulloa, L. Farias, R. Escribano (2006), Anaerobic ammonium oxidation in the oxygen-deficient waters off northern Chile, *Limnol. Oceanogr.*, *51*(5), 2145-1256

Thunell, R. C., D. M. Sigman, F. Muller-Karger, Y. Astor, R. Varela (2004), Nitrogen isotope dynamics of the Cariaco Basin, Venezuela, *Global Biogeochem. Cycles*, *18*, GB3001, doi:10.1039/2003GB002185

Tyrell, T. (1999), The relative influence of nitrogen and phosphorus on oceanic primary production, *Nature*, *400*, 525-531

Voss, M. J., J. W. Dippner, J. P. Montoya (2001), Nitrogen isotope patterns in the oxygen deficient waters of the Eastern Tropical North Pacific Ocean, *Deep Sea Res. I, 48*(8), 35-49

Wada, E., and A. Hattori (1978), Nitrogen isotope effects in the assimilation of inorganic nitrogenous compounds by marine diatoms, *Geomicrobiology Journal*, *1*, 85-101

Wada, E. (1980), Nitrogen isotope fractionation and its significance in biogeochemical processes occurring in marine environments, *Isotope Marine Chemistry*, edited by E. Goldberg, Y. Horibe, K. Saruhashi, 375-398, Uchida Rokakuho, Toyko

Waser, N. A. D., P. J. Harrison, B. Nielson, S. E. Calvert, D.H. Turpin (1998), Nitrogen isotope fractionation during the uptake and assimilation of nitarte, nitrite, ammonium, and urea by a marine diatom, *Limno. and Oceanogr.*, *43*(2), 215-224

Wu, J., S. E. Calvert, C. S. Wong (1997), Nitrogen isotope variations in the northeast subarctic Pacific: Relationships to nitrate utilization and trophic structure, *Deep Sea Res. I*, *44*, 287-314

Yoshikawa, C., Y. Yamanaka, T. Nakatsuka (2006), Nitrate-Nitrogen Isotopic Patterns in Surface Waters of the Western and Central Equatorial Pacific, *J. Oceanogr., 62*, 511-525

Zickfeld, K., M. Eby, and A.J. Weaver (2008), Carbon-cycle feedbacks of changes in the Atlantic meridional overturning circulation under future atmospheric CO2, *Global Biogeochem. Cycles*, *22*(3), GB3024, doi 10.1029/2007GB003118

Appendices

Appendix A: Anisotropic Viscosity Scheme

Horizontal viscosity is required in ocean circulation models to resolve the western boundary currents and to smooth out numerical noise [*Munk*, 1950; *Bryan et al.*, 1975; *Large et al.*, 2001]. Isotropic viscosity schemes apply one large viscosity value needed for these purposes everywhere in the model which is not physically realistic outside of these specific areas. A major deficiency when using isotropic viscosities is the underestimation of the Pacific Equatorial Undercurrent which in models is typically about 10% compared to what is observed [*Large et al.*, 2001]. The Pacific Equatorial Undercurrent is a source of relatively warm, fresh, nutrient-poor and oxygen-rich water that flows into the Eastern Pacific which has significant physical and biogeochemical effects. We implement an anisotropic viscosity scheme similar to *Large et al.* [2001] in the tropics to better resolve equatorial dynamics. Figure A1 shows zonal and meridional surface viscosities used and Figure A2 shows a comparison at 125°W of the simulated currents with observations in the Eastern Tropical Pacific [*Kessler*, 2006], the region most significantly affected by the anisotropic viscosity scheme.

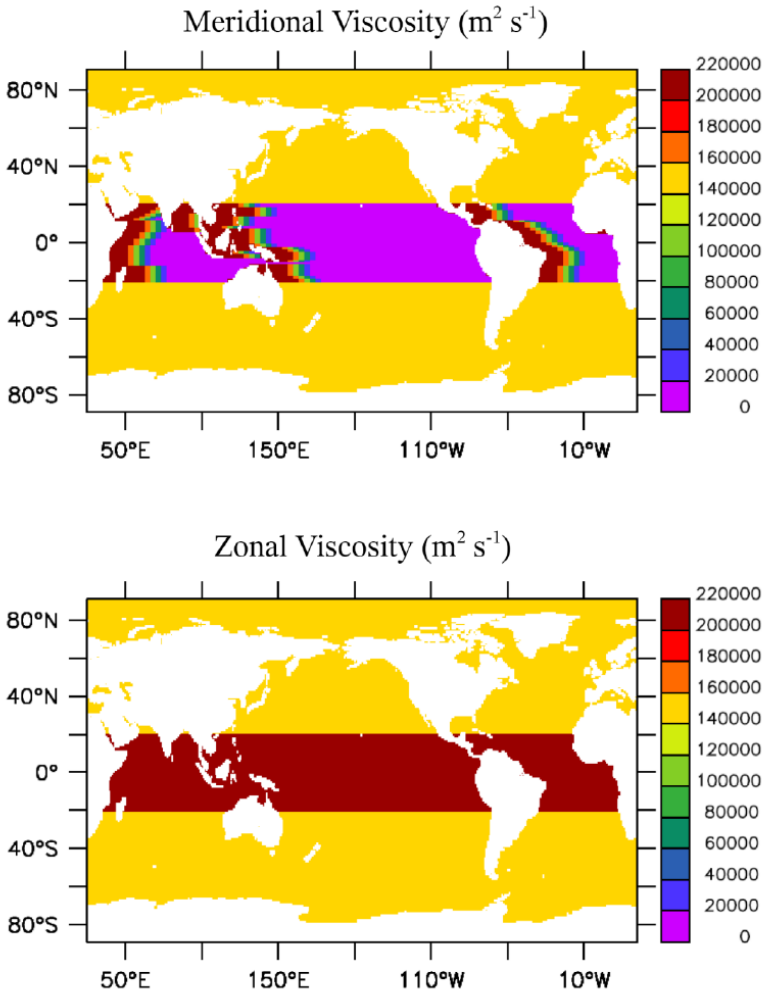

Figure A1. Surface viscosity in the meridional and zonal directions.

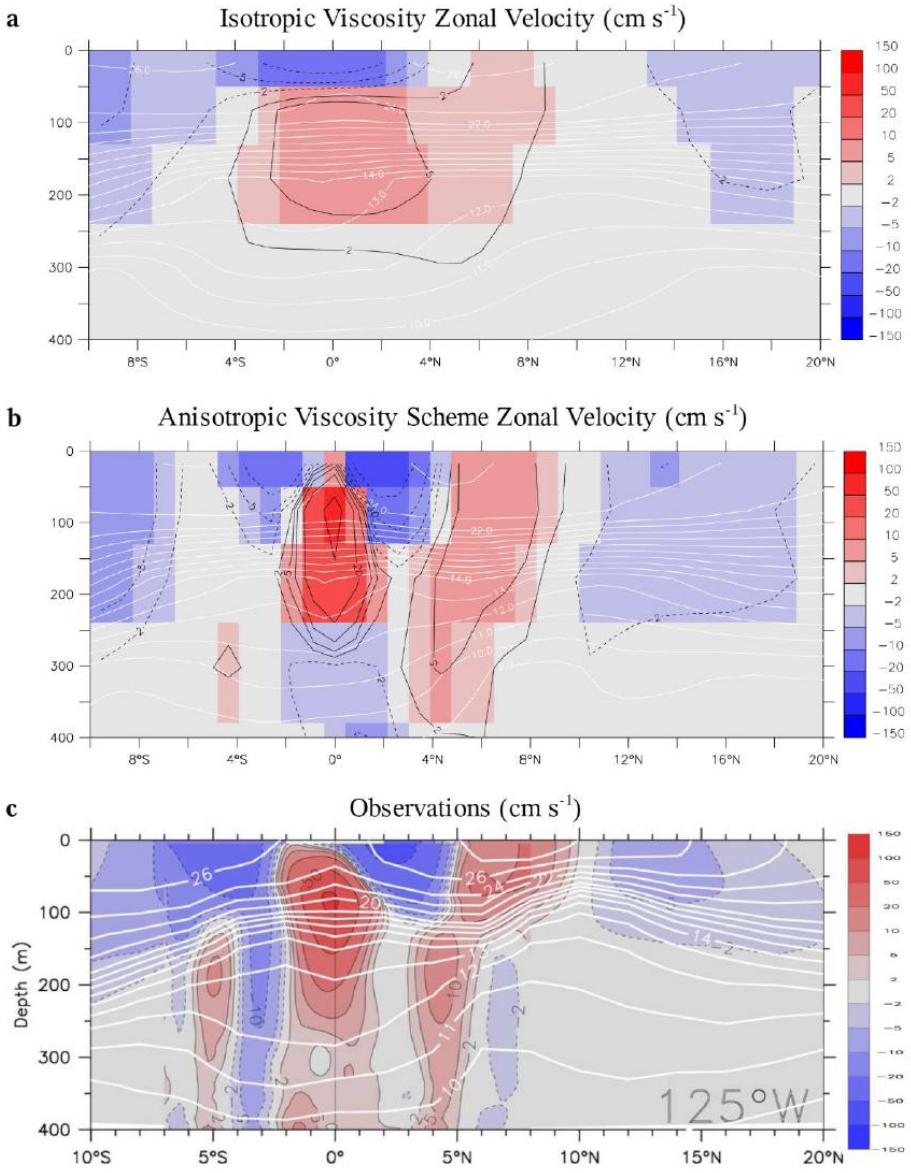

Figure A2. Annual averaged zonal velocity (cm s^{-1}) along 125°W using (a) an isotropic viscosity, (b) the anisotropic viscosity scheme and (c) observations from *Kessler* [2006].

Appendix B: The Marine Ecosystem Model

This appendix provides a description of the parameters used in the full set of time-dependent equations in the marine ecosystem model (See Table B1). It suffices to note that the equations for total nitrogen ($^{14}N + {}^{15}N$) ecosystem variables are identical to the ones of ^{15}N if $R_X = \beta_X/(1+\beta_X) = 1$, which are located in Appendix C.

The function J_O provides the growth rate of non-diazotrophic phytoplankton, determined from irradiance (I), NO_3^-, and PO_4^{3-},

$$J_O(I, NO_3^-, PO_4^{3-}) = \min(J_{OI}, J_{Omax}u_N, J_{Omax}u_P) \quad \text{(B1)}$$

The maximum growth rate is dependent only on temperature (T):

$$J_{Omax} = a \bullet \exp(T / T_b) \quad \text{(B2)}$$

such that growth rates increase by a factor of ten over the temperature range of -2 to 34 °C. We use a=0.11 d^{-1} for the maximum growth rate at 0 °C which was determined to optimize surface nutrient concentrations. Under nutrient-replete conditions, the light-limited growth rate J_{OI} is calculated according to:

$$J_{OI} = \frac{J_{Omax}\alpha I}{\left[J_{O\max}^2 + (\alpha I)^2\right]^{1/2}} \quad \text{(B3)}$$

where α is the initial slope of the photosynthesis vs. irradiance (P-I) curve. The calculation of the photosynthetically active shortwave radiation *I* and the method of averaging equation (B3) over one day is outlined in *Schmittner et al.* [2005]. Note this version does not include in the correction for the error in the calculation of light limitation that has been recently discovered [*Schmittner et al.*, 2008b]. Nutrient limitation is represented by the product of J_{Omax} and the nutrient uptake rates, $u_N = NO_3^-/(k_N + NO_3^-)$ and $u_P = PO_4^{3-}/(k_P + PO_4^{3-})$, with $k_P = k_N R_{P:N}$ providing the respective nutrient uptake rates.

Diazotrophs grow according to the same principles as the general phytoplankton class, but are disadvantaged in nitrate-bearing waters by a lower maximum growth rate, J_{Dmax}, which is set to zero below 15°C:

$$J_{Dmax} = c_D \max[0, a(\exp(T / T_b) - 2.61] \quad \text{(B4)}$$

The coefficient c_D handicaps diazotrophs by dampening the increase of their maximal growth rate versus that of the general phytoplankton class with rising temperature. We use $c_D = 0.5$, such that the increase per °C warming of diazotrophs is 50% that of other phytoplankton. This handicap is further decreased to $c_D = 0.25$ when aeolian dissolved Fe deposition is below 10 μmol Fe m^2 yr^{-1} [*Fan et al.*, 2006] and smoothly transitions to $c_D = 0.5$ outside of these areas. However, diazotrophs have an advantage in that their growth rate is not limited by NO_3^- concentrations:

$$J_D(I, PO_4) = \min(J_{DI}, J_{Dmax} u_P) \quad \text{(B5)}$$

although they do take up NO_3^- if it is available (see term 5 in the right hand side of eq. C10). The N:P of model diazotrophs is equal to the genreral phytoplankton class (16:1). Although there is evidence that the best-studied diazotrophs of the genus *Trichodesmium* can have much higher N:P [e.g. *Sanudo-Wilhelmy et al.*, 2004], the more abundant unicellular diazotrophs are uncharacterized [*Karl et al.*, 2002] and for simplicity of interpretation we opted to keep the N:P of both phytoplankton groups identical.

The first order mortality rate of phytoplankton is linearly dependent on their concentration, P_O. DOM and the microbial loop are folded into a single fast-remineralization process, which is the product of P_O and the temperature dependent term

$$\mu_P = \mu^*_P \exp(T / T_b). \qquad \text{(B6)}$$

Diazotrophs also die at this linear mortality rate that sets the rate of remineralization in the upper water column and determines primary production. Figure B1 compares the annual rates of primary production with the Vertically Generalized Production Model (VGPM) which is based on satellite observations of chlorophyll [*Behrenfeld and Falkowski*, 1997]. The model simulates similar patterns and total magnitude as the VGPM estimate but significantly larger primary production in the equatorial upwelling regimes and smaller production in the oligotrophic subtropical gyres. However, recent estimates using dissolved O_2 isotope measurements suggests that the VGPM may be underestimating primary production by a factor of 1.3 - 3 across the Tropical Pacific Basin [*Juraneck et al.*, 2009].

Grazing of phytoplankton by zooplankton is unchanged from *Schmittner et al.* [2005]. Detritus is generated from sloppy zooplankton feeding and mortality among the three classes of plankton, and is the only component of the ecosystem model to sink. It does so at a speed of

$$w_D = \left\{ \begin{array}{c} w_{D0} + m_w z, z \le 1000m \\ w_{D0} + m_w 1000m, z > 1000m \end{array} \right\}, \quad \text{(B7)}$$

increasing linearly with depth z from w_{D0}=7 md^{-1} at the surface to 40 md^{-1} at 1 km depth and constant below that, consistent with observations [*Berelson*, 2002]. The remineralization rate of detritus is temperature dependent and decreases by a factor of 5 in suboxic waters, as O_2 decreases from 5 μM to 0 μM:

$$\mu_D = \mu_{DO} \exp(T / T_b)[0.65 + 0.35\tanh(O_2 - 6)] \quad \text{(B8)}$$

Remineralization transforms the N and P content of detritus to NO_3^- and PO_4^{3-}. Photosynthesis produces oxygen, while respiration consumes oxygen, at rates equal to the consumption and remineralization rates of PO_4, respectively, multiplied by the constant ratio $R_{O:P}$. Dissolved oxygen exchanges with the atmosphere in the surface layer (F_{sfc}) according to the OCMIP protocol.

Oxygen consumption in suboxic waters (O_2 < ~5 μM) is inhibited, according to

$$r_{sox}^{O2} = 0.5\left[\tanh\left(O_2 - 5\right) + 1\right] \quad \text{(B9)}$$

but is replaced by the oxygen-equivalent oxidation of nitrate,

$$r_{sox}^{NO3} = 0.5\left[1 - \tanh\left(O_2 - 5\right)\right]. \quad \text{(B10)}$$

Water column denitrification consumes nitrate at a rate of 80% of the oxygen equivalent rate, as NO_3^- is a more efficient oxidant on a mol per mol basis (i.e., one mol of NO_3^- can accept $5e^-$ while 1 mol of O_2 can accept only $4e^-$). It is also inhibited as NO_3^- approaches zero to avoid denitrification if NO_3^- is not readily available according to

$$l_{NO3} = 0.5[\tanh(NO_3^- - 5) + 1] \, . \quad \text{(B11)}$$

We implement the sedimentary denitrification metamodel equation of *Middleburg et al.* [1996] which parameterizes sedimentary denitrification based on the labile carbon flux (F_c) into the sediments:

$$SedDeni = \alpha_{SD} \times 10 \wedge \left[-0.9543 + 0.7662 \times \log(F_c) - 0.2350 \times \log(F_c)^2\right] \quad \text{(B12)}$$

SedDeni is the amount of NO_3^- that is removed from the bottom water. We assume that the flux of labile carbon (F_c) occurs at a ratio of $R_{C:N} = 6.6$ of the sinking nitrogen in the organic detritus. Because the continental shelves are not well resolved in the model, we use an additional parameterization for them. It is assumed that the continental shelf covers half of all ocean grid boxes at 130 m next to land grid points. Therefore, half of the sinking organic matter in these locations is also used in the sedimentary denitrification model and the remaining organic matter continues to sink. The physical circulation model's inability to fully resolve coastal upwelling systems also underestimates primary production and sinking carbon fluxes on the continental shelves and hence sedimentary denitrification. To account for this, we arbitrarily multiply the sedimentary denitrification rate by a coefficient α_{SD} tuned to 6.5 to set the global deep oceanic $\delta^{15}NO_3^-$ average in the model to ~5‰. Without this parameterization, the deep oceanic $\delta^{15}NO_3^-$ average slowly drifts well above 10‰. The tuning parameter α_{SD} was also tested at the values of 6 and 7, which resulted in deep oceanic $\delta^{15}NO_3^-$ averages of 5.2‰ and 4.95‰, respectively. Figure 2 shows the spatial distribution of sedimentary denitrification. In the model ~80% of the sedimentary denitrification occurs within this shelf parameterization.

Parameter	***Symbol***	***Value***	***Units***
Phytoplankton (P_O, P_D) Coefficients			
Initial slope of P-I curve	α	0.1	$(W\ m^{-2})^{-1}\ d^{-1}$
Photosynthetically active radiation	*PAR*	0.43	
Light attenuation in water	k_w	0.04	m^{-1}
Light attenuation through phytoplankton	k_c	0.03	m^{-1} $(mmol\ m^{-3})^{-1}$
Light attenuation through sea ice	k_i	5	m^{-1}
Maximum growth rate	a	0.13	d^{-1}
Half-saturation constant for N uptake	k_N	0.7	$mmol\ m^{-3}$
Specific mortality rate	μ_{P2}	0.025	d^{-1}
Fast recycling term (microbial loop)	μ^*_{P0}	0.02	d^{-1}
Diazotrophs' handicap	c_D	0.5	
Zooplankton (Z) Coefficients			
Assimilation efficiency	γ_1	0.925	
Maximum grazing rate	g	1.575	d^{-1}

Parameter	***Symbol***	***Value***	***Units***
Prey capture rate	ε	1.6	$(\text{mmol m}^{-3})^{-2}$ d^{-1}
Mortality	μ_Z	0.34	$(\text{mmol m}^{-3})^{-2}$ d^{-1}
Excretion	γ_2	0.05	d^{-1}
Detritus (D) Coefficients			
Remineralization rate	μ_{D0}	0.048	d^{-1}
Sinking speed at surface	w_{D0}	7	m d^{-1}
Increase of sinking speed with depth	m_w	0.04	d^{-1}
E-folding temperature of biological rates	T_b	15.65	ºC
Other Coefficients			
Molar elemental ratios	$R_{O:N}$	10.6	
	$R_{N:P}$	16	

Table B1: Marine Ecosystem Parameters.

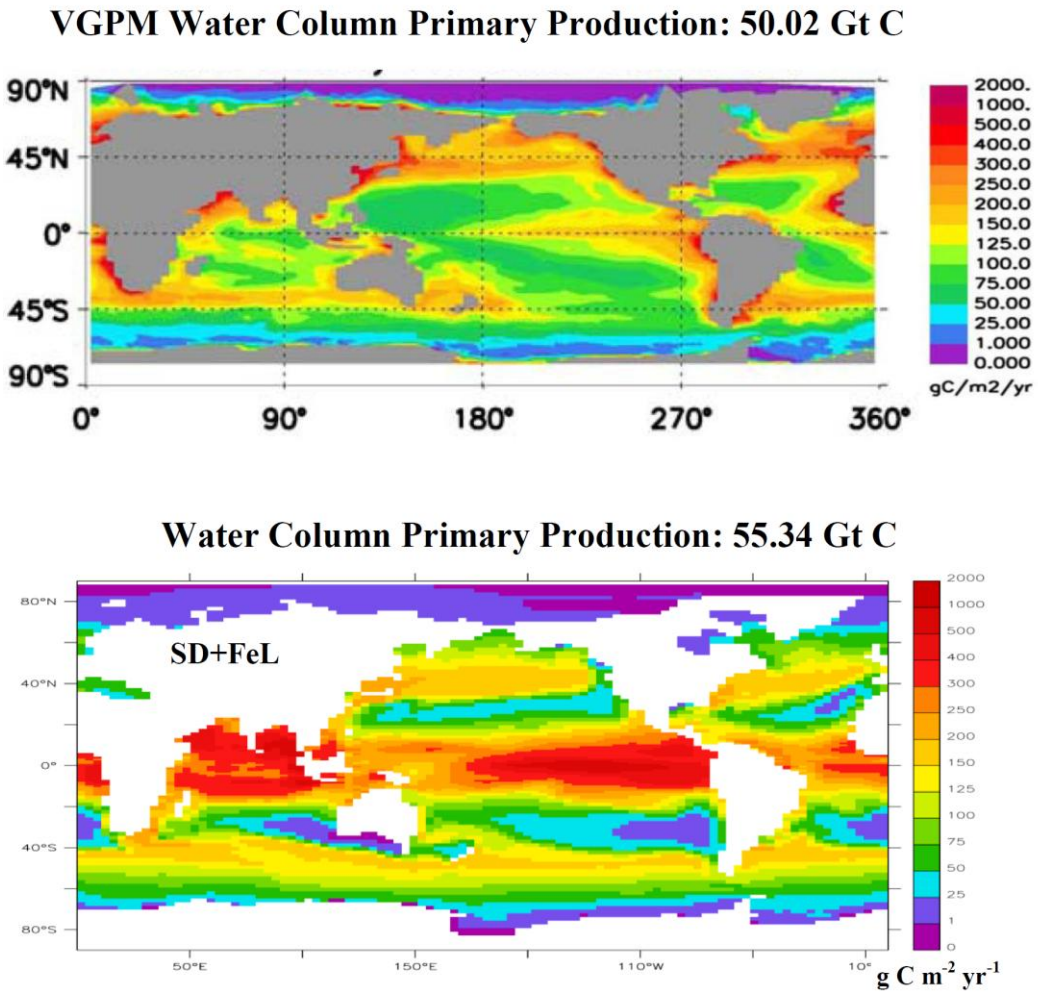

Figure B1. Comparison of annual vertically integrated primary production rates of the (top) VGPM estimate [*Behrenfeld and Falkowski*, 1997] and (bottom) SD+FeL model simulation.

Appendix C: The Nitrogen Isotope Model

The open system fractionation equation is used for fractionation during algal NO_3^- assimilation [*Altabet and Francois*, 2001]:

$$\delta^{15}P_O = \delta^{15}NO_3^- - \varepsilon_{ASSIM}(1 - u_{NO3}), \quad \text{(C1)}$$

where $\delta^{15}P_0$ is the δ^{15}N of phytoplankton biomass assimilated during one time step, Δt, and u_{NO3} is the fraction of NO_3^- available that is converted into biomass ($u_{ASSIM} = J_O P_O \times \Delta t / NO_3^-$). When algae assimilate all available NO_3^- into their biomass (i.e. $u_{ASSIM} = 1$) they will incorporate the same δ^{15}N value as that of the source material. Many studies have estimated the fractionation factor in both laboratory and ocean environments. A wide variety of values have been reported in culture settings ranging from 0.7‰ to 23‰ [*Wada and Hattori*, 1978; *Montoya and McCarthy*, 1995; *Waser et al.*, 1998; *Neeboda et al.*, 2003; *Granger et al.*, 2004]. A more confined range has been observed in field estimates from 4‰ to 15‰ [*Wada*, 1980; *Altabet et al.*, 1991; *Altabet and Fracois*, 1994; *Wu et al.*, 1997; *Altabet et al.*, 1999; *Sigman et al.*, 1999; *Altabet and Francois*, 2001; *Karsh et al.*, 2003; *DiFiore et al.*, 2006; *Needoba et al.*, 2006] . In our model we choose a constant value of 5‰ which is near the majority of estimates, although it is important to bear in mind the uncertainty in the parameter choice and the possibility that it varies in space and time.

Nitrate in suboxic waters have been observed to have much higher δ^{15}N values due to fractionation during denitrification. Observations from present day suboxic zones in the Eastern Tropical North Pacific (ETNP) and the Arabian Sea (AS) have reported fractionation factors ranging from 22-30‰ [*Cline and Kaplan*, 1975; *Liu and Kaplan*, 1989; *Brandes et al.*, 1998; *Altabet et al.*, 1999; *Voss et al.*, 2001; *Sigman et*

al., 2003], we adopt a value of 25‰ in the model. Note that because these estimates were derived from field studies in which the isotope effect was estimated from the total nitrogen loss, they implicitly include the effect of anammox [*Galbraith et al.*, 2008]. Fractionation during denitrification is also simulated using the open system fractionation equation

$$\delta^{15}NO_3^{OX} = \delta^{15}NO_3^- - \varepsilon_{WCD}(1 - u_{NO3}), \quad \text{(C2)}$$

where NO_3^{OX} is the oxygen-equivalent reduction of nitrate converted into N_2 gas during denitrification. The term u_{DENI} is the fraction of available NO_3^- which is reduced into N_2 gas ($u_{NO3} = \mu_D D$ x *0.8* x $R_{O:N}$ x r^{NO3}_{sox} x L_{NO3} x Δt / NO_3^-).

Excretion is the process responsible for the step-wise enrichment of $\delta^{15}N$ along the trophic chain in our model and is simulated using the instantaneous fractionation equation:

$$\delta^{15}NO_3^- = \delta^{15}Z - \varepsilon_{EXCR}. \quad \text{(C3)}$$

The instantaneous fractionation equation is used because excretion will always be a small fraction of the total zooplankton biomass and has been measured to be consistently depleted by ~6‰ relative to its body [*Montoya*, 2008], which is the source of the excreted nitrogen. This leads to the average enrichment of ~3.4 per trophic level [*Minagawa and Wada*, 1984].

Implementing these fractionation equations into the marine ecosystem model requires us to consider the exchanges of ^{14}N and ^{15}N between the various N pools separately. Total nitrogen abundance now has the form

$$N = {}^{14}N + {}^{15}N \tag{C4}$$

for each variable in the isotope model. A fractionation coefficient is calculated for each process so the same equations for total N can be applied to ^{15}N [*Giraud et al.,* 2000]. For example, consider fractionation during algal NO_3^- assimilation. The isotopic ratio of new nitrogen biomass (P_O) is found using equations (1) and (2):

$${}^{15}P_O = \beta_{ASSIM}\,{}^{14}P_O \tag{C5}$$

where

$$\beta_{ASSIM} = \frac{{}^{15}NO_3}{{}^{14}NO_3} - \frac{\varepsilon_{ASSIM}(1-u_{NO3})R_{std}}{1000}. \tag{C6}$$

Applying equations (C4) and (C5) gives the amount of new $^{15}P_O$ relative to the amount of total new nitrogen biomass, which is given by the primary production ($J_O P_O$), calculated by the marine ecosystem model.

$$^{15}P_O = \frac{\beta_{ASSIM}}{1+\beta_{ASSIM}} J_O P_O \tag{C7}$$

Analogous derivations can be done for all fractionation coefficients. The time-dependent set of equations for ^{15}N which are embedded into the marine ecosystem model are as follows:

$$\frac{\partial^{15} NO_3}{\partial t} = \left(R_D \mu_D D + \frac{\beta_{EXCR}}{1+\beta_{EXCR}} \gamma_2 Z + R_P \mu_P P_O - \frac{\beta_{ASSIM}}{1+\beta_{ASSIM}} J_O P_O \right.$$

$$\left. - \frac{\beta_{ASSIM}}{1+\beta_{ASSIM}} u_N J_D P_D \right) \times \left[1 - \frac{\beta_{WCD}}{1+\beta_{WCD}} 0.8 R_{O:N} r_{sox}^{NO3} l_{NO3} \right] \tag{C8}$$

$$\frac{\partial^{15} P_O}{\partial t} = \frac{\beta_{ASSIM}}{1+\beta_{ASSIM}} J_O P_O - R_P \mu_P P_O - R_{P_O} G(P_O) Z - R_{PO} \mu_{P2} P_O^2 \tag{C9}$$

$$\frac{\partial^{15} P_D}{\partial t} = \left(\frac{\beta_{ASSIM}}{1+\beta_{ASSIM}} u_N + \frac{\beta_{NFIX}}{1+\beta_{NFIX}} (1-u_N) \right) J_D P_D + -R_{P_D} G(P_D) Z - R_{P_D} \mu_P P_D \tag{C10}$$

$$\frac{\partial^{15} Z}{\partial t} = \gamma_1 \left[R_{P_O} G(P_O) + R_{P_D} G(P_D) \right] Z - \frac{\beta_{EXCR}}{1+\beta_{EXCR}} \gamma_2 Z - R_Z \mu_Z Z^2 \tag{C11}$$

$$\frac{\partial^{15}D}{\partial t} = (1-\gamma_1)\left[R_{P_O}G(P_O) + R_{P_D}G(P_D)\right]Z + R_{P_D}\mu_P P_D + R_{P_O}\mu_{P2}P_O^2 + R_Z\mu_Z Z^2$$

$$-R_D\mu_D D - R_D w_D \frac{\partial D}{\partial z} \qquad \text{(C12)}$$

where $R_{N=PO,\,PD,\,Z,\,D}$ = ^{15}N / (^{14}N + ^{15}N) is the ratio of heavy over total nitrogen. The complete parameter description is provided in Appendix B. Here it suffices to note that the equations for total nitrogen (^{14}N + ^{15}N) are identical to the ones of ^{15}N except that $R_X = \beta_X/(1+\beta_X) = 1$ in the total nitrogen equations.

The model was carefully tested with zero fractionation (i.e., all enrichment factors set to zero) in order to quantify and minimize numerical errors, which can occur for example due to slightly negative values of biological tracers caused by inaccuracies of the advection scheme. The biological code was adjusted to avoid negative concentrations as much as possible. Initially numerical errors in $\delta^{15}N$ ranged from ± 1‰ in grid points at the sea floor to ± 0.1‰ in the upper ocean. Setting R_{std} = 1 instead of R_{std} = 0.0036765, the actual atmospheric N_2 isotope ratio, reduces the numerical errors by over an order of magnitude. R_{std} is set to the value 1 so both isotope variables will be on the same order of magnitude. This prevents ^{15}N from becoming very close to zero as often, where inaccuracies of the advection scheme can cause it to be negative. This modification amounts to a scaling of ^{15}N and ^{14}N by a constant factor which does not affect the $\delta^{15}N$ dynamics. The remaining numerical errors of ±0.1‰ in the deep ocean and ±0.01‰ in the upper ocean are two orders of magnitude smaller than the observed variability. The model is integrated for over 7,000 years as it approaches equilibrium.